2019 SCEC Report

Project #19097

Region-Specific Fourier-Based Site Amplification Modeling

Jeff Bayless, Andreas Skarlatoudis, Paul Somerville
AECOM, Los Angeles

Jonathan P. Stewart
University of California, Los Angeles

With special thanks to Pengfei Wang, Tristan Buckreis, and Chukwuebuka Nweke from UCLA

Table of Contents

1. Introduction

This SCEC study addresses the need for improved nonlinear site amplification models on the SCEC BBP. We infer site response in northern and southern California from earthquake recordings and develop appropriate models for frequency-dependent amplification of horizontal-component Fourier amplitude ordinates as a function of site parameter V_{s30} and the peak ground acceleration on reference rock. The bulk of this study follows the conceptual framework of Seyhan and Stewart (2014; SS14 hereafter), in which a semi-empirical site amplification model was developed for response spectra (PSA). We take similar steps using Fourier amplitude ordinates.

The proposed model supplements the available options on the SCEC BBP for site amplification. The most commonly used model at this time is one implemented by Rob Graves. This module adjusts the Fourier amplitudes of the time series simulated for rock conditions using either the Campbell and Bozorgnia (2013) or Boore et al. (2013) models. Both of these models were created for response spectra corrections even though they are being applied to Fourier amplitudes. Rob Graves has commented that this correction is acceptable when the modifications are small, even though it is not ideal.

Another amplification model from Shi et al. (2017), is ready to be implemented on the BBP and should be available soon if it is not there already. This model combines a shear wave velocity profile generator with an analytic nonlinear site response. A shortcoming of the Shi et al. (2017) model is that it has not been validated in the manner of site terms in ground motion models. A model by Hashash et al. (2018; H18 hereafter) for site amplification is also ready but, to our knowledge, has not been implemented on the BBP; this uses the Shi et al. (2017) approach with many randomized profiles to develop average amplitude and phase factors. This approach too requires validation, as encountered through similar work in the central and eastern U.S., where bias in the simulations results was encountered for some conditions (Stewart et al. 2017a).

Last year we (the AECOM PIs) set out to develop a Fourier-based site amplification model using data recorded in California and Nevada, but the model was not finalized because the observed nonlinearity was not statistically significant for critical V_{s30} bins. This is resolved in this SCEC report by including several updates to the previous approach. These include refining the analysis regions and expanding the database of recorded ground motions with those recorded since the conclusion of the NGA West2 project; these extra data have been compiled by Wang and Stewart (2019), Nweke et al. (2018) and Buckreis et al. (2019). The linear portion of the model has southern- and northern- California region-specific terms. The nonlinear portion of the model is developed from a combined database, including data from outside of California. We work with Fourier amplitude spectra (FAS) residuals from the Bayless and Abrahamson (2019; BA19 hereafter) ergodic FAS GMPE.

2. Ground Motion Data

This study makes use of the Effective Amplitude Spectrum (EAS) component of the Fourier amplitude spectrum, which is defined by PEER (Goulet et al., 2018). The EAS is the orientation-independent horizontal component FAS of ground acceleration. The EAS ordinates are smoothed using the Konno and Ohmachi (1998) smoothing window using smoothing window parameter b=188.5 (following Kottke et al, 2015). The terms FAS and EAS are used interchangeably in this report, but in all cases it is the smoothed EAS that has been analyzed and from which the model is based, unless noted otherwise.

Below, three different databases are described. To constrain the nonlinear portion of the model all three data sets are combined to create one generic model. This is done because there is not sufficient strong amplitude ground motion data (which may have been subject to soil nonlinearity) to constrain the nonlinearity on a regional basis. To develop the linear portions of the model, which uses the full range of ground motions (weak, moderate, and strong) there is sufficient data on regional scales to create region-specific models.

The primary data source is the NGA-West2 FAS database (Ancheta et al. 2014). The subset of the NGA-West2 FAS database used includes ground motions recorded from crustal earthquakes worldwide. Expanding to regions outside of the US was necessary in order to constrain the nonlinearity in the residuals. This database is described in Bayless and Abrahamson (2019). Figure 1 shows a magnitude-distance scatterplot of the data used at f=10 Hz.

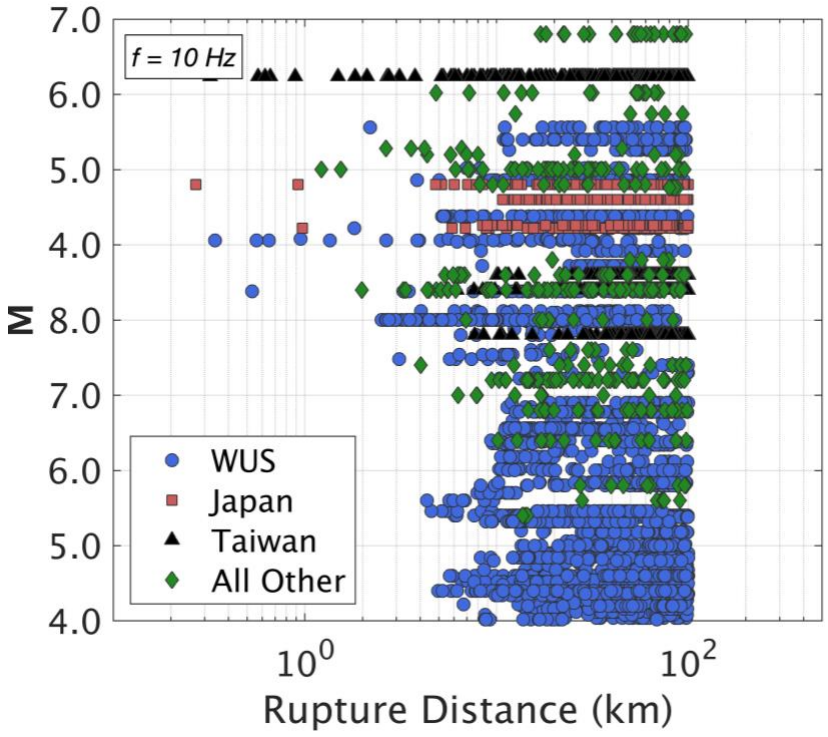

Figure 1. Magnitude-distance scatterplot of the FAS data used from the NGA-West 2 database.

The second database, developed by Wang and Stewart (2019), extends the NGA-West2 database with earthquakes and recordings in California and northern Mexico since 2011. This database includes 29 new events with 6,584 three-component ground motion recordings. Each of the three-component records has been processed by Wang and Stewart (2019) according to

standard protocols developed during Pacific Earthquake Engineering Research center (PEER)-NGA projects, as described in Ancheta et al. (2014). The FAS have been processed following the procedure described in Kishida et al. (2016). Figure 2 shows a map of the recording stations from this supplemental database.

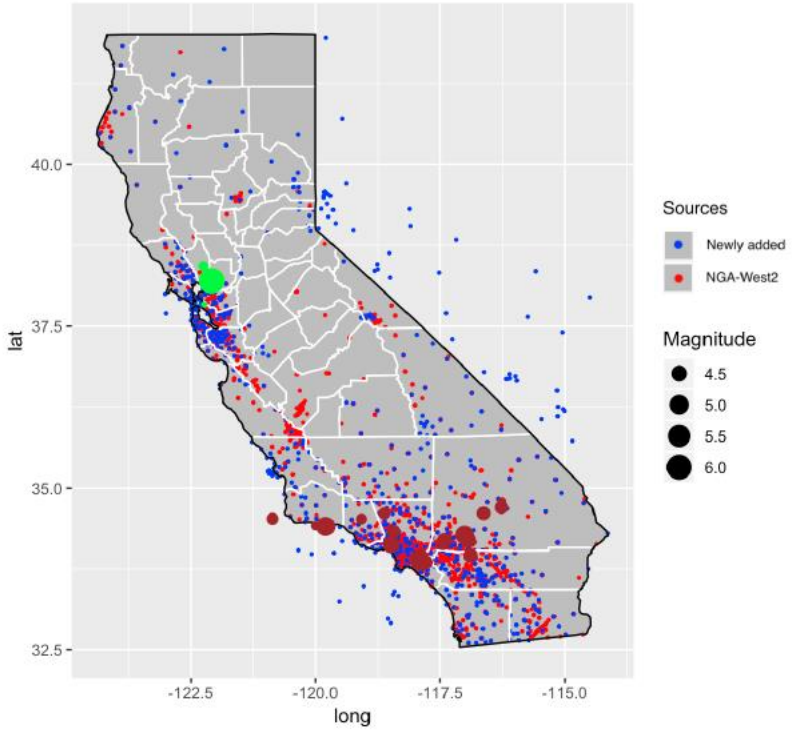

Figure 2. Map of California showing locations of earthquakes and recording stations from the Wang and Stewart (2019) database. Figure reproduced from Wang and Stewart (2019).

The third database, compiled by Buckreis et al. (2019), further supplements the NGA-West2 data, mostly with recordings in central and northern California. This database includes 39 events (5 already existing in NGA-West2 and 34 new additions) with 3,721 new three-component ground motion recordings. Each of the three-component records has been processed by Buckreis et al. (2019) according to the same PEER protocols, and the FAS and smoothed EAS have been calculated as part of the current study.

3. Procedure

3.1 Model Formulation

Our analysis of site terms from empirical data follows the procedures in Seyhan and Stewart (2014) and Stewart et al. (2017) using FAS from observations and predictions from the Bayless and Abrahamson (2019) FAS model. The observed site response of the FAS is termed F_S in natural log units. These site effects, which have uncertainty, are used as the "observations" to which the scaling relation is fit, as described in the next section. The F_S can be partitioned as

$$F_S = F_{lin} + F_{nl} \quad (1)$$

where F_{lin} and F_{nl} are the linear and nonlinear site amplification components in natural log units as predicted from an ergodic model. These two amplification components are modeled by Equations 2 and 3, where f_0, f_1, f_2, and f_3 are model parameters, and IM_{ref} is taken as the peak ground acceleration (PGA) for the reference site condition (PGA_r). V_c is the limiting V_{s30} beyond which there is no further linear site amplification scaling, and V_{ref} is the reference V_{s30} condition for which the amplification is taken as unity.

$$F_{lin} = f_0 \ln\left(\frac{\min(V_{s30}, V_c)}{V_{ref}}\right) \quad (2)$$

$$F_{nl} = f_1 + f_2 \ln\left(\frac{IM_{ref} + f_3}{f_3}\right) \quad (3)$$

The nonlinear term is formulated to decrease the overall amplification for strong shaking levels (quantified through the PGA_r) and to have no effect for weak PGA_r levels. This is achieved by setting parameter f_3 to 0.1 g and f_1 to 0. We use $V_{ref} = 760$ m/s and $V_c = 1000$ m/s following Seyhan and Stewart (2014) and Bayless and Abrahamson (2019), respectively. The model parameter f_2 is formulated as a function of the parameter V_{s30} and the frequency-dependent model coefficients f_4 and f_5, and constants V_a and V_b. The form of Equation 4 is the same as from Seyhan and Stewart (2014), Chiou and Youngs (2008) and Hashash et al. (2018).

$$f_2 = f_4[\exp\{f_5(\min\{V_{s30}, V_a\} - V_b)\} - \exp\{f_5(V_a - V_b)\}] \quad (4)$$

3.2 Model Building

Following the SS14 approach, the nonlinear model is formed on the basis of interpreting the behavior of the data, in this case using the complete NGA-West 2 database (screened for quality) along with the supplemental data. We examine the nonlinearity of the site amplification first, using FAS residuals from the reference condition GMM binned by the parameter V_{s30} and plotted against input peak acceleration. Once the nonlinear model is developed, the linear portion of the site amplification is determined on a regional basis and is compared with the BA19 linear model for all of California.

Nonlinear Scaling

At each of a set of log-spaced frequencies the analysis is performed independently. First, data is selected based on quality, source-to site rupture distance (0-300 km), region as needed, number of recordings per earthquake (5 minimum), and with the requirement that PGA_r > 0.01g. Then, residuals are calculated from the BA19 GMM for the V_{s30} = 760 m/s site condition. These residuals are partitioned into event terms and within-event residuals using a nonlinear mixed effects regression. The recorded PGA is converted to PGA_r using the linear BSSA14 site amplification model, and for each of a set of V_{s30} bins, we plot within-event residuals versus PGA_r, get least squares fit to Equation 3. The standard error and confidence intervals of the

coefficient f_2 are recorded. Finally, we plot the coefficients f_2 versus V_{s30} and get least squares fit to the nonlinear Equation 4. This yields the model parameters f_4 and f_5 which are smoothed in frequency space to develop the final model.

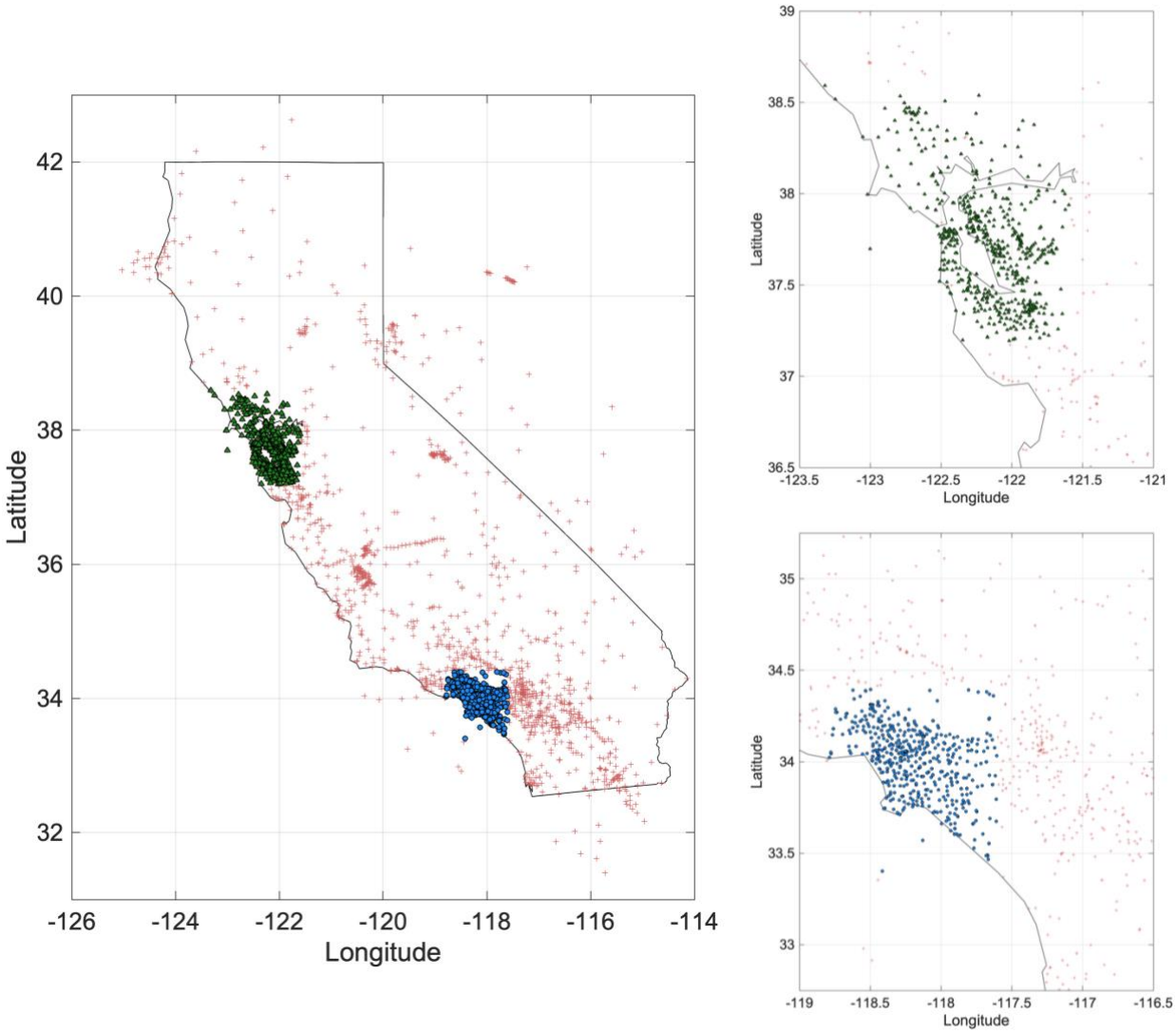

Figure 3. Left: a map of the recording stations in proximity to California used to build the nonlinear model (red, green, and blue), the linear model for the Bay Area region (green) and the linear model for the Los Angeles region (blue). Right: insets of the two regions.

Linear V_{s30} Scaling

Once the nonlinear portion is determined, the remaining within-event residuals are partitioned by region and the mixed-effects regression is performed to get the linear V_{s30}-based site amplification (coefficient f_0 from Equation 2). Based on the available data, and because the BA19 model is developed for all of California, we decided to build distinct linear models for the Bay Area and Los Angeles regions. The data for the Bay Area region includes recording stations with Latitudes between 37.1 and 38.6 degrees, and Longitudes between -122.6 and -121.6 degrees. The data for the Los Angeles region includes recording stations with Latitudes between 33.4 and 34.4 degrees, and Longitudes between -118.8 and -117.6 degrees. The recording stations used at 5 Hz are mapped in Figure 3. The number of ground motion

recordings and number of earthquakes used in the regression versus frequency are shown in Figure 4.

It is recognized that regional variations of anelastic attenuation can potentially introduce bias in a regional residual analysis, which could also potentially be mapped into the regional site amplification. This is addressed by defining the spatial extent of each region to be small enough, and to use data with small enough source-to-site rupture distances (<80 km initially, then expanded to <150 km), such that anelastic attenuation effects should be insignificant. This assumption is verified in the residual analyses in the next section.

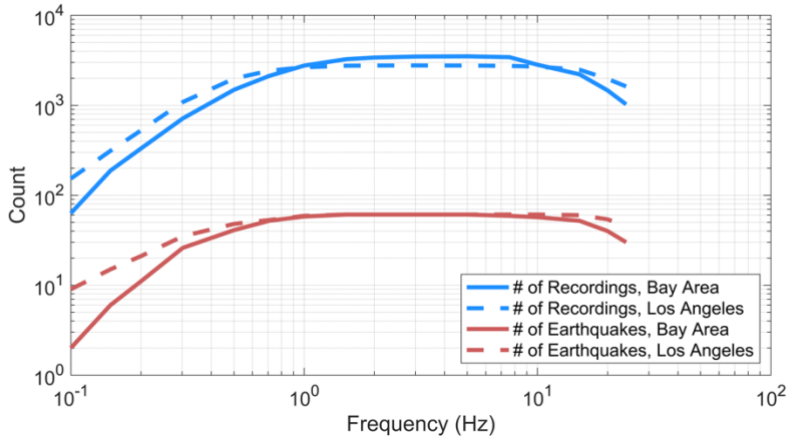

Figure 4. The number of ground motion recordings and unique earthquakes used in the regression for the linear $\boldsymbol{V_{s30}}$ scaling models at each frequency, by region.

4. Results

4.1 Nonlinear Scaling

To investigate nonlinearity, the EAS within-event residuals are compiled within bins of V_{s30} (≤ 200, 200–310, 310–520, 520–760, ≥ 760 m/s), which are plotted against PGA_r. Figure 5 shows these results for frequencies of 0.3, 1.0, 5.0, 10.0, and 20.0 Hz. Following the approach of SS14, we get the least-squares regression to fit the data to the form of Equation 3 (solid red lines in Figure 5). The black symbols in Figure 5 represent the residual binned means with 95% confidence intervals. The coefficient f_2, which exhibits V_{s30} bin dependence, represents the slope of this nonlinear fit to the residuals. Larger negative values represent larger reduction in residuals (e.g. model over-predictions) for large ground motions (characterized by the PGA_r). Within each panel of Figure 5 the estimates of coefficient f_2 are given, along with the confidence intervals and standard error of this coefficient.

SS14 judged their estimates of coefficient f_2 to be statistically significant when the absolute value of f_2 was larger than its standard error and came up with two conclusions:

> *(1) nonlinearity decreases with increasing V_{S30}, generally becoming statistically insignificant for relatively stiff sites; and (2) nonlinearity decreases as period increases, being statistically significant only for T ≤ ~1 s, except for the softest soil sites (V_{S30} < 200 m/s).*

Using the same benchmark for statistical significance, our conclusions are generally consistent with those from SS14. We find the apparent nonlinearity is strongest for the lowest V_{s30} bins and for higher frequencies. The coefficient f_2 estimates are generally not statistically significant at frequencies below 1 Hz. For the V_{s30} ≥ 760 m/s bin, there is significantly less data (manifested by the very wide confidence intervals in mean binned residuals) and the trends in the residuals versus PGA_r are not systematic, therefore we judge the f_2 estimates shown in Figure 5 to be inconsequential for this V_{s30} bin. At all frequencies, the apparent nonlinearity for V_{s30} bins 310–520 and 520–760 m/s is weak or nonexistent. For V_{s30} bins ≤ 200 and 200-310 m/s, the apparent nonlinearity increases with increasing frequency and is statistically significant for frequencies greater than about 0.5 Hz.

With estimates of the coefficient f_2 in hand for each V_{s30} bin and frequency, we then examine the dependence of f_2 on these two parameters. Figure 6 shows the V_{s30} and frequency dependence of f_2, where the red symbols are the coefficients estimated from the previous step, and the error bars show the 95% confidence intervals in these estimates. As in previous studies (e.g. Seyhan and Stewart, 2014; Chiou and Youngs; 2008 and Hashash et al., 2018) f_2 is modeled using the form of Equation 4. This model is shown by the solid red lines in Figure 6. As with SS14, we elected to not allow the model to produce positive values of f_2. Below 0.5 Hz, we constrain the f_2 model to be zero, based on the observed statistical significance in the previous step. $V_a = 500$ and $V_b = 300$ (Equation 4) are selected based on visual interpretation of the slope coefficients, where V_a is the V_{s30} beyond which f_2 approaches zero.

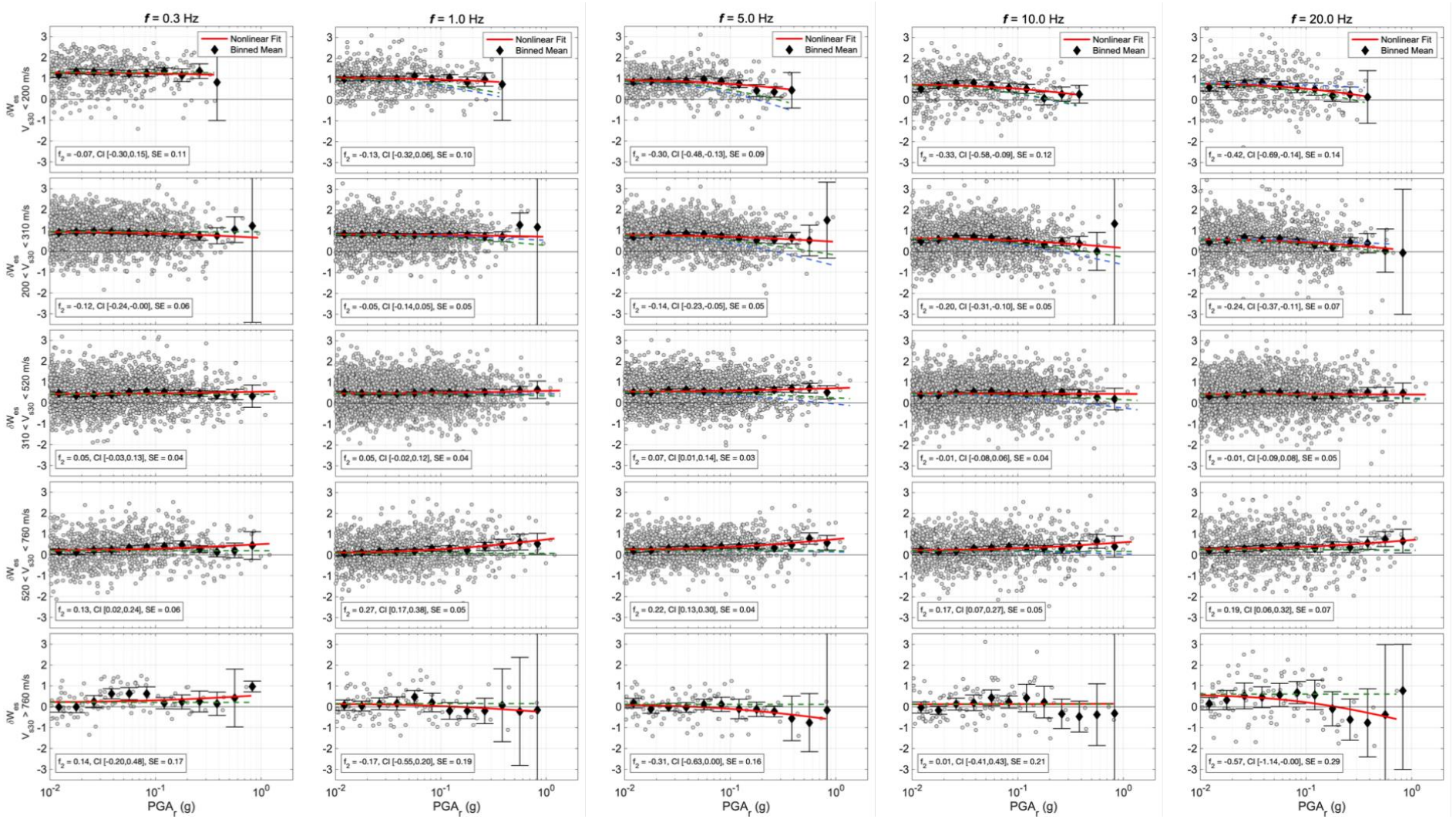

Figure 5. Variation of within-event residuals from the rock condition EAS GMPE versus peak ground acceleration on rock, binned by V_{s30} (rows) and for five frequencies (columns). The red line is the nonlinear fit to the residuals (Equation 2) and the blue and green dashed lines are the nonlinear models by Hashash et al., (2018) and Seyhan and Stewart (2014). The black diamonds represent the residual binned means with 95% confidence intervals.

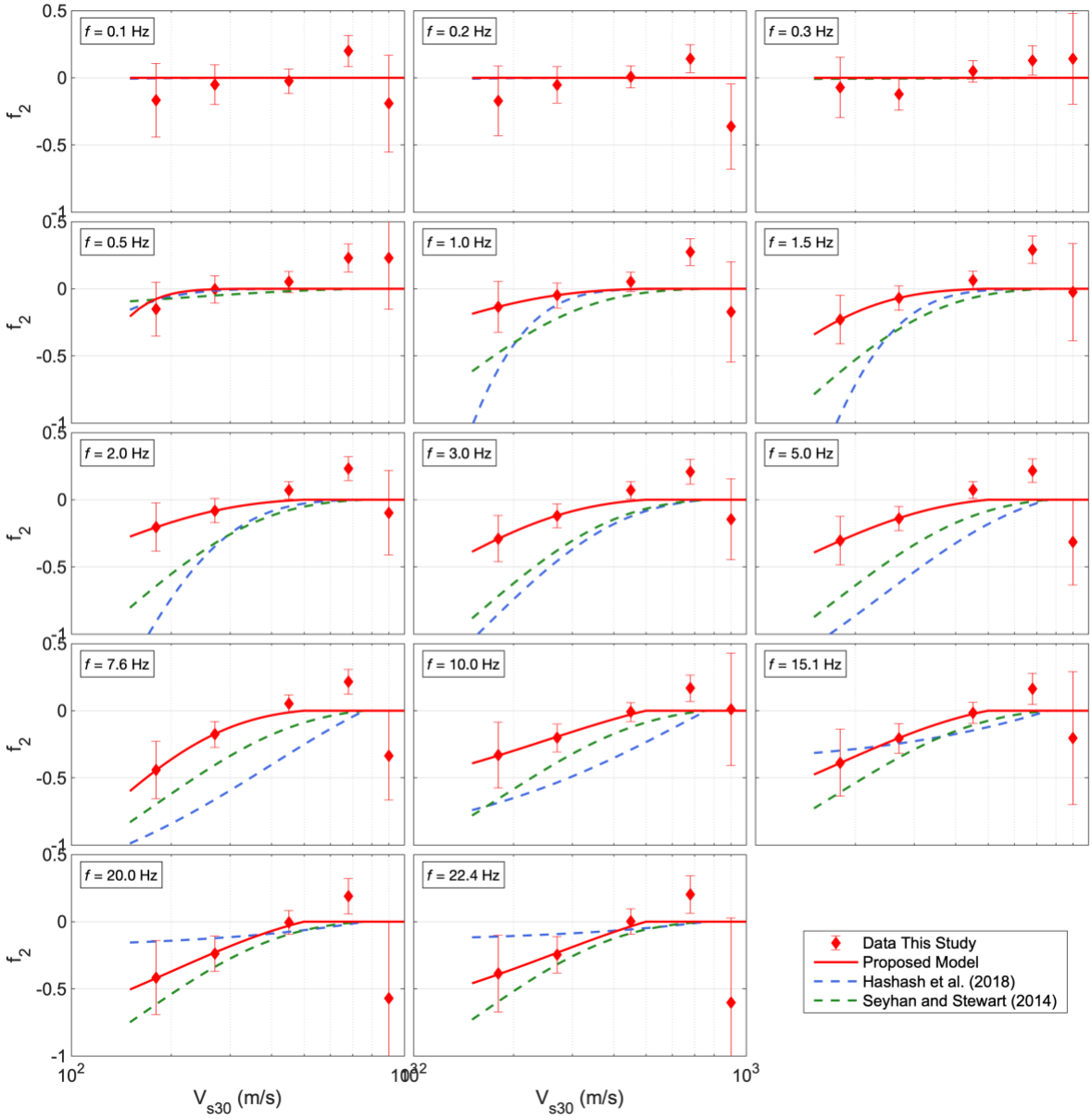

Figure 6. The V_{s30} and frequency dependence of f_2, where the red symbols are the coefficients previously estimated, the error bars show the 95% confidence intervals in these estimates, and the proposed model (Equation 4) is shown by the solid red lines. Coefficients from Seyhan and Stewart, 2014 (green) and Hashash et al., 2018 (blue) are shown.

For comparison purposes, two other nonlinear model slope coefficients are shown as identified in the legend of Figure 6: SS14 (for response spectra) and H18 (for unsmoothed FAS). H18 is a purely analytical model, created by performing large-scale 1D site response simulations of input rock motions propagated through soil columns. At frequencies below 15 Hz, both models have stronger slope coefficients for the full range of V_{s30}. Starting at 15 Hz, the proposed model slope lands somewhere between these two models. Therefore, the present model suggests generally weaker nonlinear effects than both SS14 and H18, except at the highest frequencies, where the proposed model exhibits stronger nonlinearity than H18 but weaker nonlinearity than SS14. For

frequencies between 1-15 Hz, the proposed model also has milder V_{s30} dependence and approaches zero at $V_{s30} = 500$ m/s instead of $V_{s30} = 760$ m/s.

Figure 7 shows the frequency dependence of the smoothed model coefficients $\boldsymbol{f_4}$ and f_5 (Equation 4). Tables of all model coefficients are given in Tables 1 and 2 (Appendix A). Figure 8 shows the model predictions of F_{nl} for a range of frequency, PGA_r and V_{s30}.

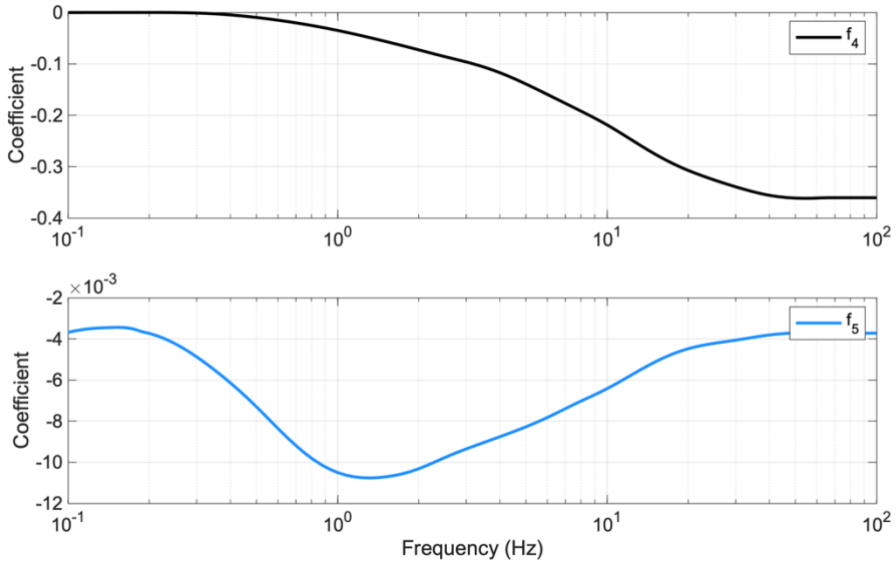

Figure 7. Frequency dependence of the nonlinear model coefficients.

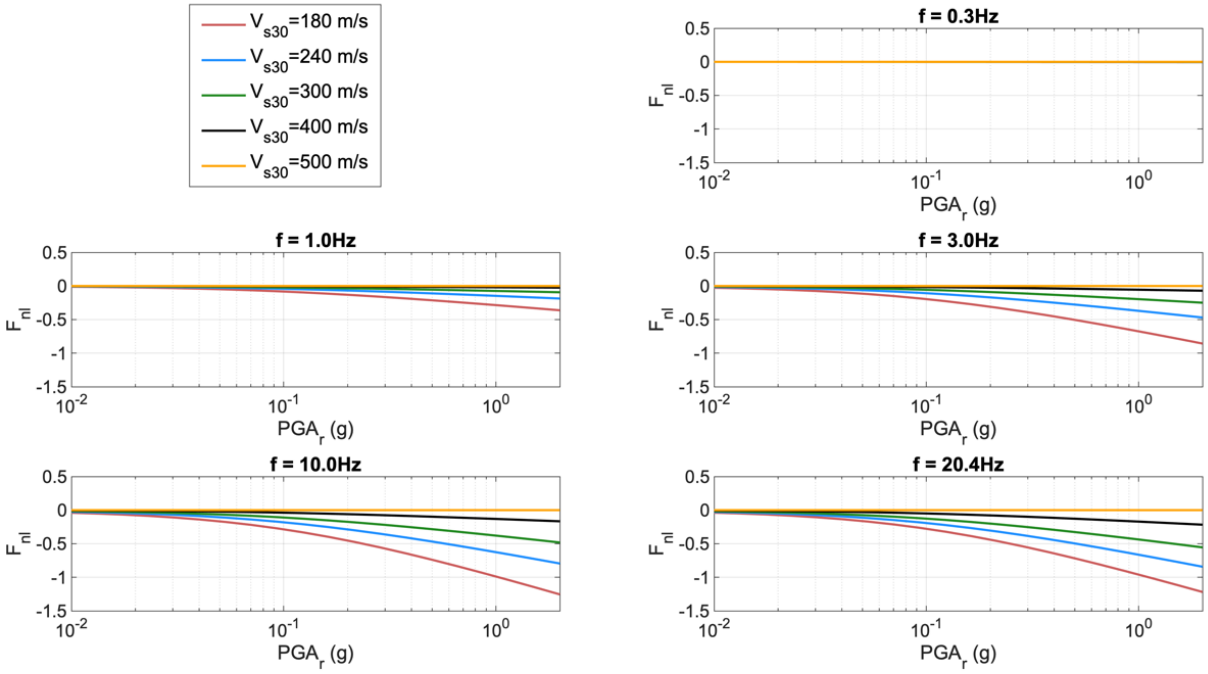

Figure 8. Model predictions of $\boldsymbol{F_{nl}}$ (ln units) for a series of frequencies and $\boldsymbol{V_{s30}}$, versus $\boldsymbol{PGA_r}$.

4.2 Regionalized Linear V_{s30} Scaling

As described in Section 3, the linear site response is modeled using the remaining within-event residuals after correcting for nonlinearity. This is achieved by regressing the residuals using Equation 2 to obtain estimates of the linear site amplification slope parameter f_0. This is repeated separately using data within the Los Angeles and Bay Area regions (defined in Section 3.2) and again with all available data in the proximity of California (Figure 3).

Figure 9 shows the Los Angeles region within-event residuals at 1 Hz for rock site conditions in blue, plotted versus V_{s30} in the left column and versus R_{rup} in the right column. In red, the residuals are shown after the regression for f_0. At 1 Hz, the linear trend in the rock residuals (top left in Figure 9) is readily apparent, and the fit to these is shown by the black dashed line.

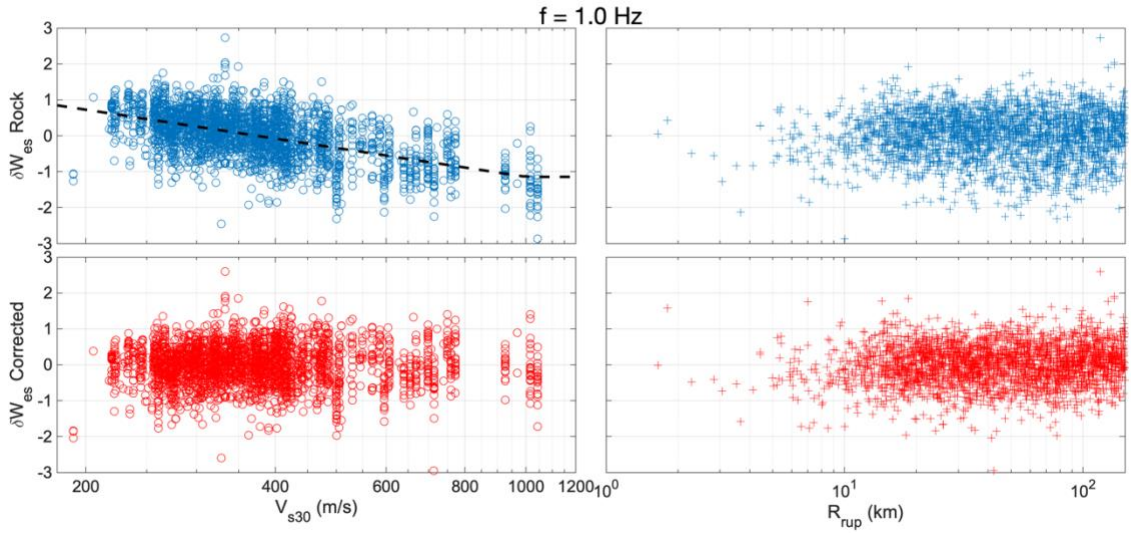

Figure 9. Within-event residuals for rock conditions (blue) and after regressing for the linear site response (red) versus $\boldsymbol{V_{s30}}$ and $\boldsymbol{R_{rup}}$. Data shown is at 1 Hz in the Los Angeles region.

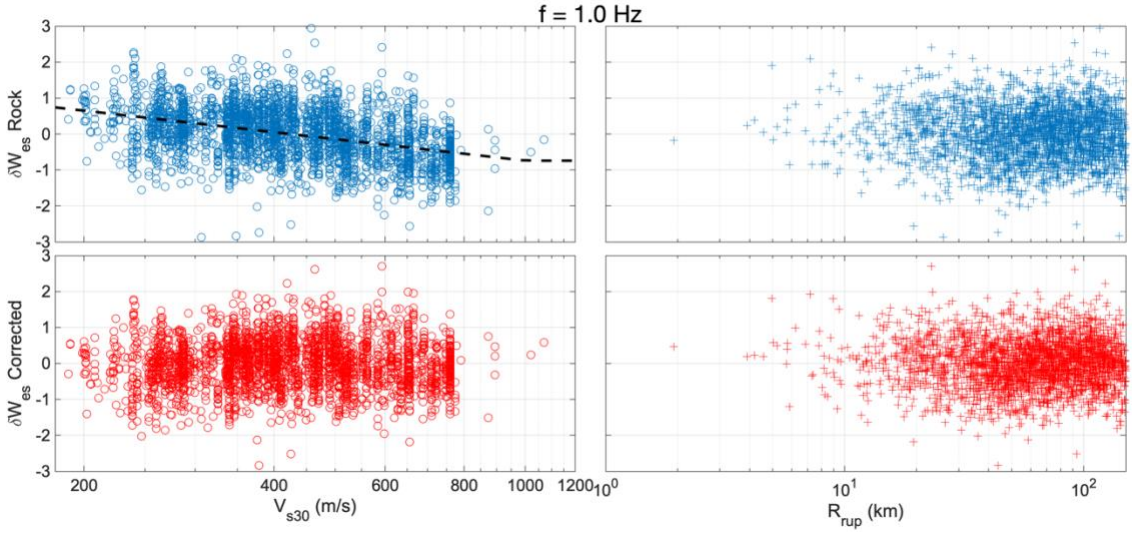

Figure 10. Within-event residuals for rock conditions (blue) and after regressing for the linear site response (red) versus $\boldsymbol{V_{s30}}$ and $\boldsymbol{R_{rup}}$. Data shown is at 1 Hz in the Bay Area region.

Generally, the residuals do not show strong trends versus rupture distance, therefore correcting for regional anelastic attenuation effects is deemed unnecessary. Based on observation of the residuals, we choose to fix $V_c = 1000$ m/s for all frequencies, as in BA19. Figure 10 shows the same results as Figure 9, but for the data in the Bay Area region.

Figure 11 shows the frequency dependence of the regionalized linear site amplification coefficients, f_0 after applying smoothing in log frequency space. This figure also shows the linear site amplification coefficient from SS14 for comparison purposes (c from Equation 2 of SS14). Tables of all model coefficients are given in Tables 1 and 2 (Appendix A).

The maximum frequency for which a regression is possible, due to the usable frequency range limitations of the data, is approximately 24 Hz. In order to provide an amplification model over the range 0.1-100 Hz, the coefficients from this study at 24 Hz are extrapolated to all higher frequencies (before smoothing.) This effectively applies the f=24 Hz amplification to the f>24 Hz ordinates.

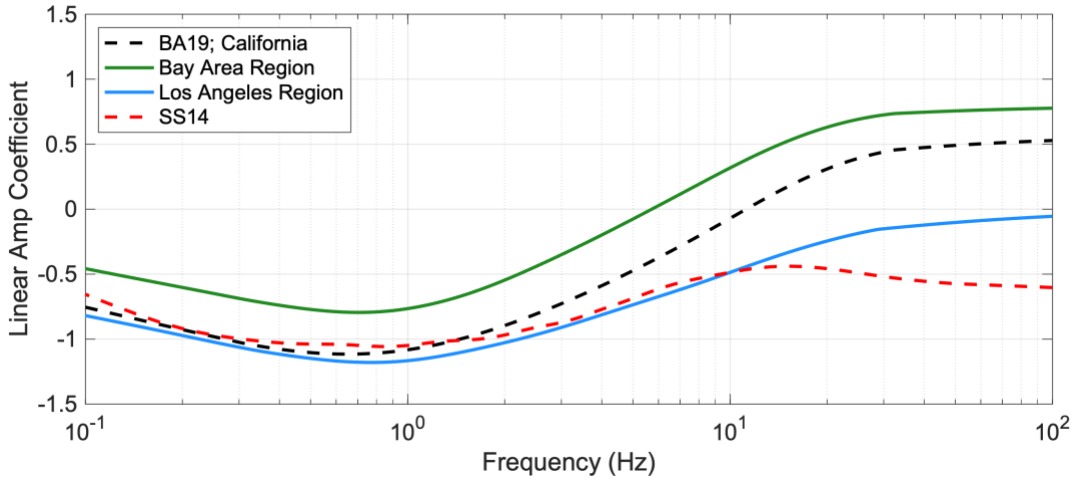

Figure 11. The frequency dependence of the linear site amplification coefficients, $\boldsymbol{f_0}$ from this study, along with the coefficient from SS14 (red dashed line; $\boldsymbol{c}$ from Equation 2 of SS14).

Observations on the Linear Scaling Coefficients

The linear site amplification term is given by Equation 2. Negative values of the coefficient f_0 (Figure 11) represent amplification for V_{s30} values less than V_{ref}, and de-amplification for V_{s30} values greater than V_{ref}. Conversely, positive values of this coefficient represent de-amplification of the ground motions for low V_{s30} values and amplification for high V_{s30} values. For the data within the Bay Area, this coefficient crosses from negative to positive values at about 6 Hz (e.g. the positive slope shown in Figure 12). This behavior is an interesting result worth discussing because it contrasts most linear V_{s30} scaling models, which predict amplification of the ground motions at sites with low V_{s30}, even for high frequencies (short periods). The key difference is that most existing models have been developed for response spectra, which is the peak response from a single-degree-of-freedom (SDOF) system. The SDOF response is influenced by a range of frequencies, and the breadth of that range is dependent on the oscillator period. For short oscillator periods, where there is little energy left to resonate the oscillator, the ordinates are influenced by a very wide frequency band of the ground motion; meaning the predominant period of the ground motion dominates the short-period response.

Because of this, differences are to be expected between FAS and PSA linear site amplification models at short periods (high frequencies).

Previous FAS amplification factors (e.g. H18) have been derived from analytical ground response simulations of input rock motions propagated through soil columns. The transfer functions computed from ground response analyses have a characteristic shape. At low frequencies corresponding to wavelengths significantly greater that the profile thickness, the amplification is unity. As frequency increases, a series of peaks are encountered at the site's modal frequencies, and these peaks are generally appreciably larger than zero (in ln units). However, as frequency increases beyond the first 2-4 modal frequencies, transfer function amplitudes tend to systematically decrease, becoming negative, as a result of soil damping effects. For profiles with low V_{s30} values, the peak amplifications are at lower frequencies than profiles with high V_{s30} values. Therefore, a low V_{s30}-valued profile may feature amplification at low (resonant) frequencies and de-amplification at very high frequencies; this behavior would not be captured in a PSA-based empirical model because of the reasons described previously. This may be manifested in the FAS model as the transition to positive values of the V_{s30} scaling coefficient at high frequencies.

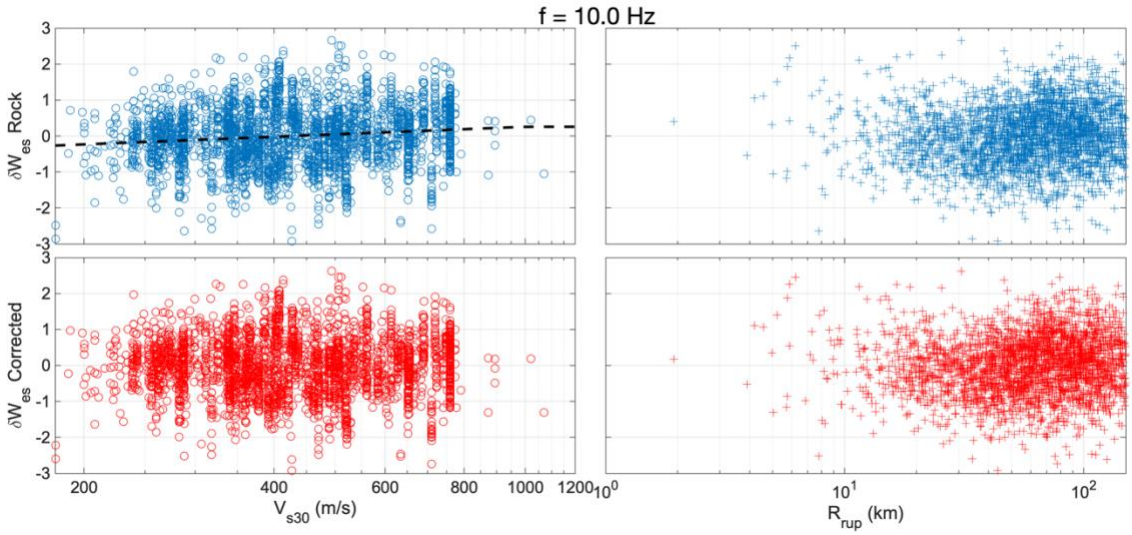

Figure 12. Within-event residuals for rock conditions (blue) and after regressing for the linear site response (red) versus $\boldsymbol{V_{s30}}$ and $\boldsymbol{R_{rup}}$. Data shown is at 10 Hz in the Bay Area region.

4.3 Model Comparisons

LA and Bay Area Models

In Figure 13, the total amplification (linear and nonlinear) is compared between the Bay Area and LA region models for a range of V_{s30} values and PGA_r. All amplification factors shown are relative to the reference V_{s30} condition of 760 m/s. Figure 11 compares the linear V_{s30} scaling coefficients for these same models.

Although the "spectral shape" of the LA and Bay Area linear V_{s30} scaling coefficients, shown in Figure 11, are similar, there are significant differences between them, which lead to substantial differences between the total amplifications in Figure 13. First, the linear part of the LA model has stronger linear amplification low frequencies and is generally more similar to the one for all of California (from BA19). This causes the total amplification (dashed lines in Figure 13) to be

the larger at low frequencies. Second, the Bay Area linear scaling coefficient crosses zero and becomes positive at about 6 Hz, where the Los Angeles linear scaling coefficient is negative for all frequencies. The change in the coefficient from negative to positive causes a change from amplification to de-amplification (for $V_{s30} < V_{ref}$) at this frequency, as discussed previously, and as manifested by the amplification factors crossing below unity for the solid lines in Figure 13. Both of these models have the same nonlinearity, which can be observed in Figure 13 as reduction in high frequency amplification for the V_{s30} = 300 m/s curves with increasing PGA_r (between panels).

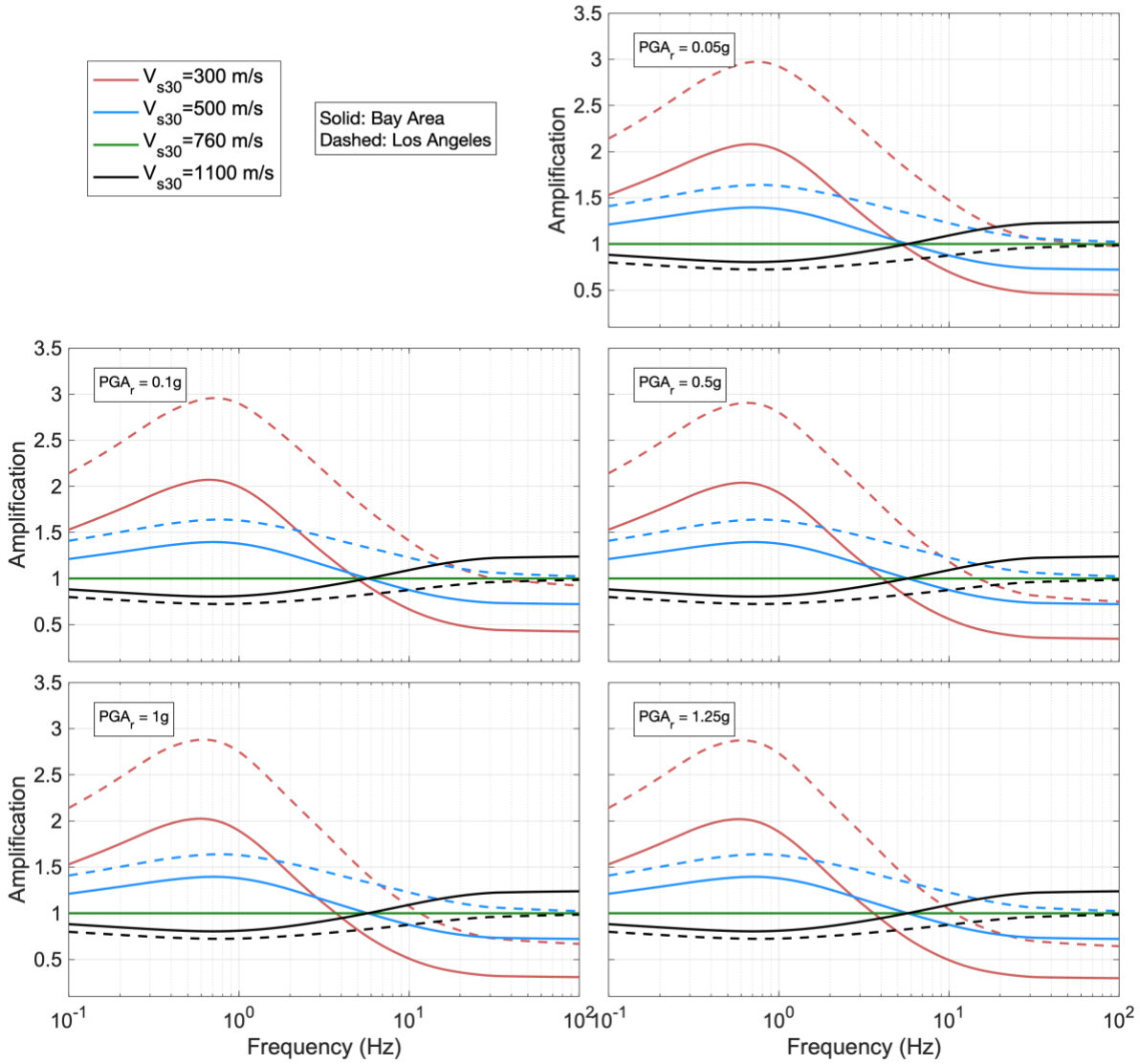

Figure 13. Total amplification (linear and nonlinear) factors for a range of $\boldsymbol{V_{s30}}$ (different colored lines as identified in the legend) and $\boldsymbol{PGA_r}$ (different panels as indicated within each.) The solid lines are for the Bay Area model, the dashed lines are for the Los Angeles region model.

Comparison with SS14

The spectral shape of the coefficients and amplification factors are similar between SS14 and the current study. All models have a similar slope in linear V_{s30} scaling coefficients between about 1 and 10 Hz. At about 15 Hz, the SS14 model coefficient peaks and then decreases. This behavior is different from the proposed model, but this difference is expected for a response spectrum-based model, in which the high frequency (short oscillator period) ordinate is controlled by the predominant frequency of the ground motion, as discussed previously. Therefore, we judge that the spectral shapes of the linear V_{s30} scaling coefficients are very consistent between these two sets of models. As a result, the total amplification factors (Figure 14) are also generally compatible for frequencies below about 10 Hz.

In SS14, the linear V_{s30} scaling coefficient remains negative for all frequencies. Additionally, SS14 studies regionalization of this coefficient and report modest variation between regions, but did find that regionalization was sensitive to data selection criteria. As discussed previously, the present model suggests generally weaker nonlinear effects than SS14. For frequencies between 1-15 Hz, the proposed model also has milder V_{s30} dependence and approaches zero at $V_{s30} = 500$ m/s instead of $V_{s30} = 760$ m/s.

Comparison with H18

The total amplification factors are compared with the Hashash et al. (2018) model in Figure 15. In Hashash et al. (2018), the site response analysis software DEEPSOIL version 6.1 (V6.1) (Hashash et al., 2016) is used to perform a large number of 1D site response simulations (30; 000+) of input rock motions propagated through soil columns representative of WUS site conditions. The amplification factors for each profile are the ratio of the output response to the input response. The Hashash et al. (2018) nonlinear analyses are conducted in the time domain using the implicit integration of the equation of motion. The soil properties in these simulations represent a range of geologic conditions in the western United States modeled as 1D profiles, with specific V_s profiles and properties from Kim et al. (2016), and seed V_s profiles for randomization from Walling et al. (2008).

Hashash et al. (2018) produced linear and nonlinear analytical site amplification models for the PSA and FAS, the model for the FAS is shown in Figure 15. This model shows a discernable difference in the amplification factors; the amplification is peaked over frequency bands which correspond to the resonant frequencies of the profiles associated with that V_{s30}. Notably, some of the Hashash et al. (2018) amplification factors, without considering the nonlinear effects, drop below unity at frequencies higher than the site's first few modal frequencies, (e.g. top right panel of Figure 15), which is in agreement with the results from this study for the Bay Area. At low frequencies, where the wavelengths are significantly longer than the profile thickness, the Hashash et al. (2018) amplification factors approach unity due to the previously discussed limitation of ground response analyses. Because of the complexity in the linear amplification factors, Hashash et al (2018) provided these factors as tables with respect to V_{s30} and soil depth, rather than a parametric model.

Comparison with Bora et al. (2019)

Figure 16 compares the total amplification factors with the linear V_{s30}-scaling component (Equation 2) of the Bora et al. (2019) FAS model. The Bora et al. (2019) model was developed using individual horizontal FAS components with high smoothing (Konno and Ohmachi, 1998 smoothing parameter b=40) from a subset of the NGA-West2 data including multiple regions. This model does not have a nonlinear component (and is not dependent on the input ground motion PGA_r), so the dotted lines in each panel of Figure 16 are identical between panels. The amplification factors from Bora et al. (2019) are quite similar to the Los Angeles model, for the

full range of V_{s30}, especially for frequencies below 15 Hz. Above 15 Hz, the Bora et al. (2019) amplifications approach unity, whereas the proposed models exhibits either amplification or de-amplification depending on the V_{s30} and PGA_r. Overall, the range of amplification factors predicted by these two models is very similar.

Comparison with Shi et al. (2017).

Shi et al. (2017) performed large scale site response simulations, similar to Hashash et al. (2018), to develop site amplification factors for the Western US. The Shi et al. (2017) simulation scheme improves on the Kamai et al. (2014) scheme in three aspects: (1) a smaller and hence more realistic variance in generating 1D random soil profiles; (2) an improved soil constitutive model that can capture the shear strength of soils; (3) use of the nonlinear method (instead of the equivalent linear method) to solve the nonlinear wave equation an to get better prediction quality at higher frequencies. At the time of writing this report we were not in possession of the Shi et al (2017) FAS amplification model so we have not compared with it, but we would like to do so in the future.

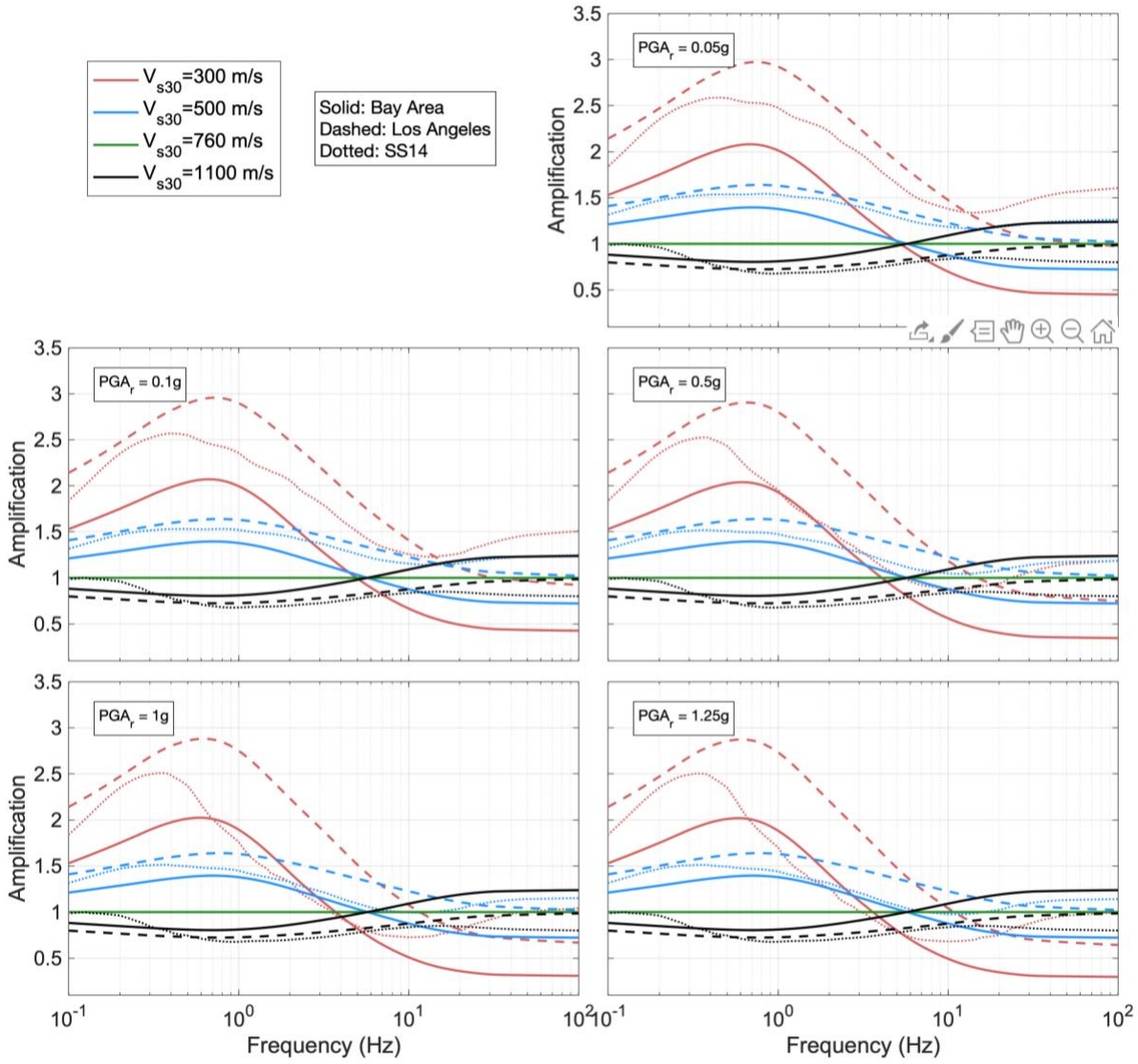

Figure 14. Total amplification (linear and nonlinear) factors compared with the SS14 model (dotted lines). The format of this figure is the same as Figure 13.

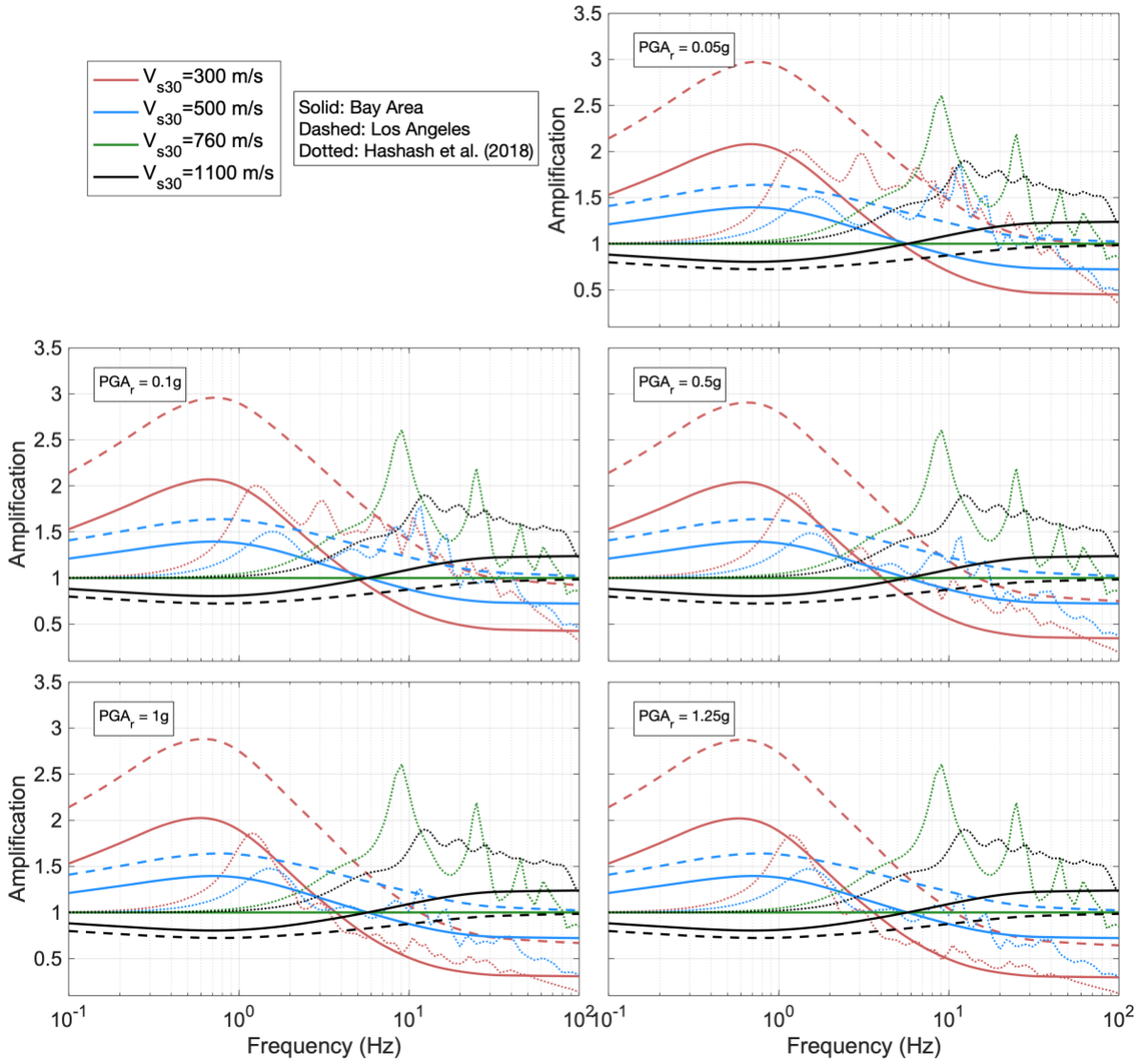

Figure 15. Total amplification (linear and nonlinear) factors compared with those from Hashash et al. (2018). The format of this figure is the same as Figure 13.

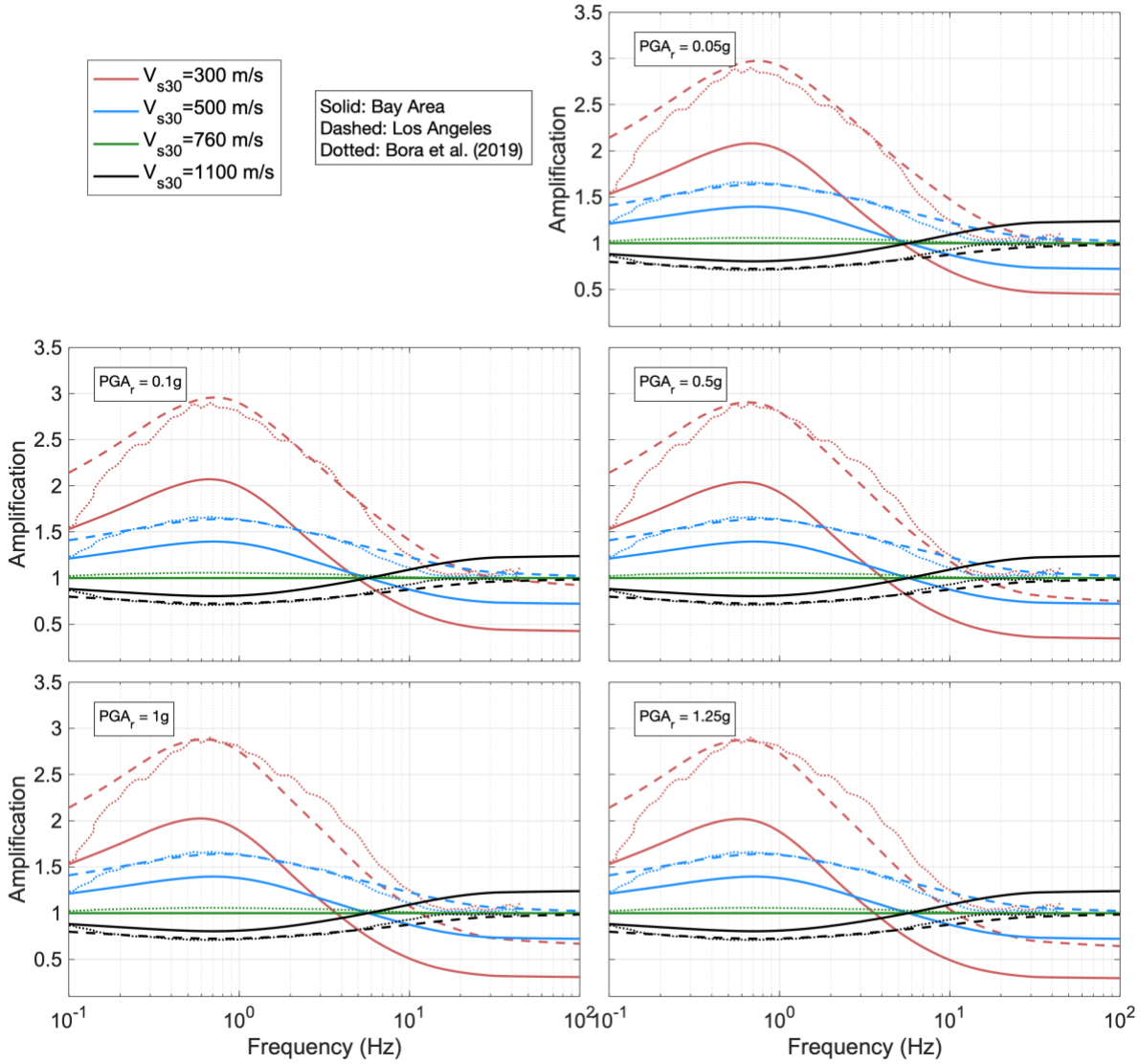

Figure 16. Total amplification (linear and nonlinear) factors compared with those from Bora et al. (2019). The format of this figure is the same as Figure 13.

4.4 Example Spectra

In Figure 17, we show an example application of the proposed models. In this figure, two scenarios are shown (**M**6 and **M**8 as identified in the legend) both for a vertical strike-slip fault with $Z_{tor} = 0$ km, and a site with $R_{rup} = 15$ km, and $V_{s30} = 360$ m/s. For both scenarios, the dotted curves show the BA19 EAS for the reference site condition (no explicit V_{s30} scaling) and the solid and dashed curves show the effects of the Bay Area and Los Angeles site amplification models, respectively, on spectral shape. The smoothing applied to the model coefficients leads to smooth EAS adjustment factors in frequency space.

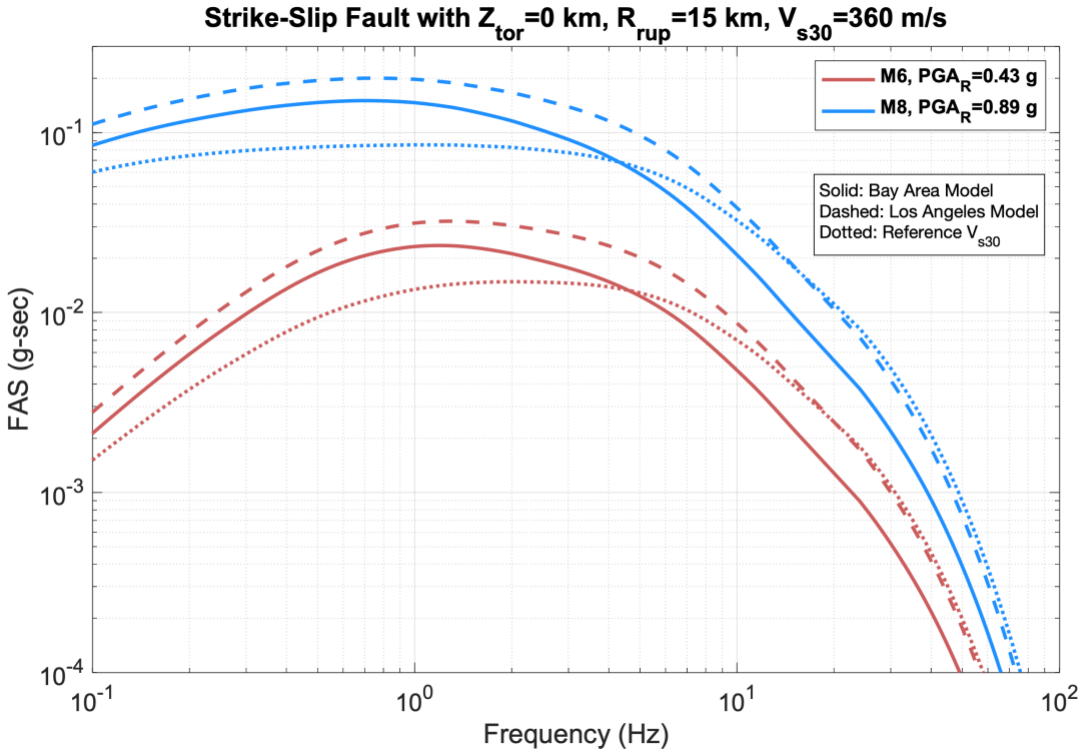

Figure 17. Example EAS spectra illustrating the effect of the proposed site amplification models on spectral shape.

5. Conclusions

We present a complete FAS site amplification model (V_{s30} scaling and nonlinearity) which is developed from ground motion recordings and is dependent on the V_{s30}, PGA_r, region, and frequency. The procedure used to infer the nonlinear site amplification from the data residuals is motivated by Seyhan and Stewart (2014). The model is applicable over the frequency range 0.1-100 Hz and the V_{s30} range 180-1500 m/s, although it is not well constrained for V_{s30} values greater than 1000 m/s. The model coefficients were extrapolated between 24-100 Hz in order to provide a broadband model. This modification applies the f=24 Hz amplification to the f>24 Hz ordinates, but care should be taken when using the model at f>24 Hz. The model does not have magnitude or distance dependence.

The nonlinear term decreases the overall amplification for strong shaking levels (quantified through the PGA_r). The FAS data analysis implies slightly weaker V_{s30} dependence of the nonlinear reduction in FAS amplification than two other similar models: SS14 and H18.

Overall, the linear V_{s30} scaling models compare favorably with other empirically-based models (e.g. Bora et al. 2019; Seyhan and Stewart, 2014); especially at low frequencies. The Hashash et al. (2019) model is most different because it features peaks in amplification over distinct frequency bands which correspond to resonance with the modal frequencies of the V_s profile.

The data analysis implies considerable regional variations in the linear V_{s30} scaling. Based on our results, the Los Angeles region has stronger linear V_{s30} scaling of FAS than the Bay Area region at low frequencies. The model previously developed for all of California (BA19) falls between these two. Additionally, the Bay Area model features de-amplification (for low V_{s30} values) of the high frequency ground motions with respect to the $V_{s30} = 760$ m/s condition. Neither the Los Angeles nor the SS14 linear V_{s30} scaling suggests de-amplification for low V_{s30} and high frequencies. The cause of this difference may be rooted in the fundamental differences between response spectra and FAS at high frequencies; the FAS is capable of capturing the peak in the site response transfer function encountered at a site's modal frequencies where the PSA is less suited to do so. We also hypothesized that this difference is related to the mapping of basin effects in the Bay Area data; for which less $Z_{1.0}$ information was available in the supplemental data, and therefore the basin depth scaling was unity for much of the data in the residual analysis. This could potentially be mapped into the event terms, which may affect the V_{s30} scaling. However, the event terms were confirmed to have no strong trends with $Z_{1.0}$, therefore we do not think this is biasing the results. The different behavior in site amplification between the Bay Area and Los Angeles regions is an excellent topic for further research.

Tables with the model coefficients can be found in Appendix A. A MATLAB function which implements the model is available for download in Appendix B.

6. References

Ancheta, TD, RB Darragh, JP Stewart, E Seyhan, WJ Silva, BS-J Chiou, KE Wooddell, RW Graves, AR Kottke, DM Boore, T Kishida, and JL Donahue (2014). NGA-West2 database, *Earthquake Spectra*, **30**, 989-1005.

Bayless J, and Abrahamson N.A. (2019) Summary of the BA18 Ground-Motion Model for Fourier Amplitude Spectra for Crustal Earthquakes in California, Bull. Seismol. Soc. Am., 109 (5): 2088-2105. doi: 10.1785/0120180238.

Boore, D.M., J.P. Stewart, E. Seyhan, and G.M. Atkinson (2014). NGA-West 2 equations for predicting PGA, PGV, and 5%-damped PSA for shallow crustal earthquakes, Earthquake Spectra 30, 1057-1085

Bora, S. S., F. Cotton, and F. Scherbaum (2019). NGA-West2 empirical Fourier and duration models to generate adjustable response spectra, Earthq. Spectra 35, no. 1, 61–93.

Bozorgnia, Y, NA Abrahamson, L Al Atik, TD Ancheta, GM Atkinson, JW Baker, A Baltay, DM Boore, KW Campbell, BS-J Chiou, R Darragh, S Day, J Donahue, RW Graves, N Gregor, T Hanks, IM Idriss, R Kamai, T Kishida, A Kottke, SA Mahin, S Rezaeian, B Rowshandel, E Seyhan, S Shahi, T Shantz, W Silva, P Spudich, JP Stewart, J Watson-Lamprey, K Wooddell, and R Youngs, 2014. NGA-West 2 research project, *Earthquake Spectra*, **30**, 973-987.

Buckreis et al (2019). Supplemental Ground Motion Database for Northern California. Personal Communication.

Campbell, KW and Y Bozorgnia (2014) NGA-West2 Ground Motion Model for the Average Horizontal Components of PGA, PGV, and 5% Damped Linear Acceleration Response Spectra. Earthquake Spectra: August 2014, Vol. 30, No. 3, pp. 1087-1115.

Hashash, Y. M. A., M. I. Musgrove, J. A. Harmon, D. R. Groholski, C. A. Phillips, and D. Park (2016). DEEPSOIL V6.1, User Manual, University of Illinois at Urbana-Champaign, Urbana, Illinois, 137 pp.

Hashash, Y.M.A., Harmon, J., Ilhan, O., Stewart, J.P., Rathje, E.M., Campbell, K.W., Silva, W.J., and Goulet, C.G. (2018). Modelling of Site Amplification via Large Scale Nonlinear Simulations with applications to North America, paper presented to the Geotechnical Earthquake Engineering and Soil Dynamics Conference, 2018.

Kamai, R., N. A. Abrahamson, and W. J. Silva (2014), Nonlinear horizontal site amplification for constraining the NGA-West2 GMPEs, Earthquake Spectra, 30 (3), 1223-1240.

Kim, B., Y. M. A. Hashash, J. P. Stewart, E. M. Rathje, J. A. Harmon, M. I. Musgrove, K. W. Campbell, and W. J. Silva (2016). Relative differences between nonlinear and equivalent-linear 1D site response analyses, Earthq. Spectra 32, no. 3, 1845–1865.

Kishida, T., Ktenidou, O., Darragh, R.B., Silva, W.J. (2016). Semi-Automated Procedure for Windowing Time Series and Computing Fourier Amplitude Spectra for the NGA-West2 Database. PEER Report No. 2016/02, Pacific Earthquake Engineering Research Center, University of California, Berkeley, CA.

Konno, K. and Ohmachi, T., (1998). Ground-motion characteristics estimated from spectral ratio between horizontal and vertical components of microtremor, Bull. Seismol. Soc. Am. 88: 228−241. 58

Kottke A., Rathje E., Boore D.M., Thompson E., Hollenback J., Kuehn N., Goulet C.A., Abrahamson N.A., Bozorgnia Y., Der Kiureghian A., Silva W.J., Wang X. (2015). Selection of random vibration procedures for the NGA East Project, PEER report, in preparation.

Nweke, CC, Wang, P, Brandenberg, SJ, and JP Stewart (2018). Reconsidering basin effects in ergodic site response models. Proc. SMIP2018 Seminar on Utilization of Strong Motion Data, Sacramento, CA

Seyhan, E., and Stewart, J. P. (2014). Semi-empirical nonlinear site amplification from NGAWest2 data and simulations, Earthquake Spectra 30, 1241–1256

Shi, J., Asimaki, D., and Graves, R.W. (2017). Sensitivity to Nonlinear Site Amplification Factors to the Models Used to Simulate and Constrain Rare Events. Report to USGS, Grant No. G17AP00042.

Stewart, JP, GA Parker, JP Harmon, GM Atkinson, DM Boore, RB Darragh, WJ Silva, and YMA Hashash, 2017a. Expert panel recommendations for ergodic site amplification in central and eastern North America, *PEER Report 2017/04*, Pacific Earthquake Engineering Research Center, Berkeley, CA.

Stewart, JP, K Afshari, CA Goulet, 2017b. Non-ergodic site response in seismic hazard analysis, *Earthquake Spectra*, **33**, 1385-1414.

Walling, M., W. Silva, and N. Abrahamson (2008). Nonlinear site amplification factors for constraining the NGA models, Earthq. Spectra 24, no. 1, 243–255.

Wang, P. and Stewart, JP, 2019. Non-Ergodic Site Response from California Ground Motion Recordings and its Predictability. A report on research conducted with support from the California Strong Motion Instrumentation Program and the US Geological Survey. Civil & Environmental Engineering Department University of California, Los Angeles

Appendix A: Model Coefficients

Table 1. Constant model coefficients.

Parameter	f_1	f_3	V_c (m/s)	V_{ref} (m/s)	V_a (m/s)	V_b (m/s)
Value	0.0	0.1	1000	760	500	300

Table 2. Frequency dependent model coefficients.

Frequency (Hz)	f_4	f_5	f_0 Bay Area	f_0 Los Angeles	f_0 California
0.1000	-5.417E-05	-3.681E-03	-4.580E-01	-8.198E-01	-7.548E-01
0.1023	-4.595E-05	-3.654E-03	-4.629E-01	-8.247E-01	-7.607E-01
0.1047	-3.773E-05	-3.628E-03	-4.678E-01	-8.297E-01	-7.665E-01
0.1072	-2.951E-05	-3.601E-03	-4.727E-01	-8.346E-01	-7.723E-01
0.1096	-2.311E-05	-3.580E-03	-4.775E-01	-8.396E-01	-7.782E-01
0.1122	-1.677E-05	-3.559E-03	-4.824E-01	-8.446E-01	-7.840E-01
0.1148	-1.043E-05	-3.538E-03	-4.872E-01	-8.496E-01	-7.898E-01
0.1175	-5.846E-06	-3.523E-03	-4.921E-01	-8.546E-01	-7.956E-01
0.1202	-1.380E-06	-3.509E-03	-4.969E-01	-8.596E-01	-8.014E-01
0.1230	3.087E-06	-3.494E-03	-5.018E-01	-8.646E-01	-8.072E-01
0.1259	5.848E-06	-3.485E-03	-5.066E-01	-8.696E-01	-8.130E-01
0.1288	8.438E-06	-3.477E-03	-5.114E-01	-8.746E-01	-8.188E-01
0.1318	1.103E-05	-3.468E-03	-5.162E-01	-8.797E-01	-8.246E-01
0.1349	1.262E-05	-3.463E-03	-5.210E-01	-8.847E-01	-8.304E-01
0.1380	1.406E-05	-3.458E-03	-5.258E-01	-8.898E-01	-8.361E-01
0.1413	1.551E-05	-3.454E-03	-5.306E-01	-8.949E-01	-8.419E-01
0.1445	1.686E-05	-3.449E-03	-5.354E-01	-9.000E-01	-8.476E-01
0.1479	1.818E-05	-3.445E-03	-5.402E-01	-9.051E-01	-8.533E-01
0.1514	1.950E-05	-3.440E-03	-5.450E-01	-9.102E-01	-8.591E-01
0.1549	1.871E-05	-3.443E-03	-5.498E-01	-9.153E-01	-8.648E-01
0.1585	1.744E-05	-3.447E-03	-5.545E-01	-9.205E-01	-8.705E-01
0.1622	1.618E-05	-3.451E-03	-5.593E-01	-9.256E-01	-8.762E-01
0.1660	2.132E-05	-3.469E-03	-5.641E-01	-9.308E-01	-8.819E-01
0.1698	2.818E-05	-3.490E-03	-5.688E-01	-9.360E-01	-8.876E-01
0.1738	3.505E-05	-3.511E-03	-5.736E-01	-9.412E-01	-8.932E-01
0.1778	4.726E-05	-3.548E-03	-5.784E-01	-9.464E-01	-8.989E-01
0.1820	6.119E-05	-3.591E-03	-5.832E-01	-9.516E-01	-9.046E-01
0.1862	7.511E-05	-3.634E-03	-5.879E-01	-9.568E-01	-9.102E-01
0.1905	8.209E-05	-3.668E-03	-5.927E-01	-9.620E-01	-9.158E-01
0.1950	8.646E-05	-3.699E-03	-5.975E-01	-9.672E-01	-9.215E-01
0.1995	9.084E-05	-3.730E-03	-6.023E-01	-9.725E-01	-9.271E-01
0.2042	8.831E-05	-3.768E-03	-6.071E-01	-9.777E-01	-9.327E-01
0.2089	8.277E-05	-3.810E-03	-6.119E-01	-9.830E-01	-9.383E-01
0.2138	7.724E-05	-3.851E-03	-6.167E-01	-9.882E-01	-9.439E-01
0.2188	6.100E-05	-3.900E-03	-6.215E-01	-9.934E-01	-9.495E-01

0.2239	3.940E-05	-3.952E-03	-6.263E-01	-9.987E-01	-9.551E-01
0.2291	1.781E-05	-4.004E-03	-6.311E-01	-1.004E+00	-9.607E-01
0.2344	-1.833E-05	-4.062E-03	-6.359E-01	-1.009E+00	-9.662E-01
0.2399	-6.277E-05	-4.125E-03	-6.408E-01	-1.014E+00	-9.718E-01
0.2455	-1.072E-04	-4.187E-03	-6.456E-01	-1.019E+00	-9.773E-01
0.2512	-1.698E-04	-4.256E-03	-6.504E-01	-1.025E+00	-9.829E-01
0.2570	-2.443E-04	-4.328E-03	-6.553E-01	-1.030E+00	-9.884E-01
0.2630	-3.187E-04	-4.400E-03	-6.601E-01	-1.035E+00	-9.940E-01
0.2692	-4.145E-04	-4.477E-03	-6.650E-01	-1.040E+00	-9.995E-01
0.2754	-5.262E-04	-4.558E-03	-6.698E-01	-1.045E+00	-1.005E+00
0.2818	-6.378E-04	-4.639E-03	-6.746E-01	-1.050E+00	-1.011E+00
0.2884	-7.746E-04	-4.724E-03	-6.795E-01	-1.055E+00	-1.016E+00
0.2951	-9.324E-04	-4.813E-03	-6.842E-01	-1.060E+00	-1.022E+00
0.3020	-1.090E-03	-4.901E-03	-6.890E-01	-1.065E+00	-1.027E+00
0.3090	-1.275E-03	-4.993E-03	-6.936E-01	-1.070E+00	-1.032E+00
0.3162	-1.487E-03	-5.088E-03	-6.981E-01	-1.074E+00	-1.037E+00
0.3236	-1.698E-03	-5.182E-03	-7.025E-01	-1.079E+00	-1.042E+00
0.3311	-1.938E-03	-5.280E-03	-7.069E-01	-1.084E+00	-1.046E+00
0.3388	-2.208E-03	-5.380E-03	-7.111E-01	-1.088E+00	-1.050E+00
0.3467	-2.478E-03	-5.479E-03	-7.154E-01	-1.093E+00	-1.055E+00
0.3548	-2.777E-03	-5.581E-03	-7.195E-01	-1.097E+00	-1.059E+00
0.3631	-3.110E-03	-5.686E-03	-7.236E-01	-1.101E+00	-1.063E+00
0.3715	-3.444E-03	-5.790E-03	-7.277E-01	-1.105E+00	-1.067E+00
0.3802	-3.804E-03	-5.897E-03	-7.316E-01	-1.109E+00	-1.071E+00
0.3890	-4.203E-03	-6.007E-03	-7.355E-01	-1.113E+00	-1.074E+00
0.3981	-4.601E-03	-6.117E-03	-7.393E-01	-1.116E+00	-1.078E+00
0.4074	-5.025E-03	-6.229E-03	-7.430E-01	-1.120E+00	-1.081E+00
0.4169	-5.489E-03	-6.344E-03	-7.467E-01	-1.124E+00	-1.084E+00
0.4266	-5.952E-03	-6.459E-03	-7.503E-01	-1.127E+00	-1.087E+00
0.4365	-6.436E-03	-6.575E-03	-7.538E-01	-1.131E+00	-1.090E+00
0.4467	-6.958E-03	-6.696E-03	-7.571E-01	-1.134E+00	-1.093E+00
0.4571	-7.480E-03	-6.816E-03	-7.604E-01	-1.137E+00	-1.096E+00
0.4677	-8.019E-03	-6.939E-03	-7.636E-01	-1.141E+00	-1.098E+00
0.4786	-8.593E-03	-7.065E-03	-7.667E-01	-1.144E+00	-1.101E+00
0.4898	-9.168E-03	-7.191E-03	-7.697E-01	-1.147E+00	-1.103E+00
0.5012	-9.756E-03	-7.318E-03	-7.725E-01	-1.150E+00	-1.105E+00
0.5129	-1.038E-02	-7.449E-03	-7.753E-01	-1.153E+00	-1.107E+00
0.5248	-1.099E-02	-7.579E-03	-7.779E-01	-1.155E+00	-1.109E+00
0.5370	-1.163E-02	-7.711E-03	-7.803E-01	-1.158E+00	-1.110E+00
0.5495	-1.229E-02	-7.844E-03	-7.826E-01	-1.161E+00	-1.112E+00
0.5623	-1.296E-02	-7.977E-03	-7.847E-01	-1.163E+00	-1.113E+00
0.5754	-1.364E-02	-8.109E-03	-7.867E-01	-1.165E+00	-1.114E+00
0.5888	-1.435E-02	-8.241E-03	-7.885E-01	-1.168E+00	-1.115E+00
0.6026	-1.507E-02	-8.373E-03	-7.901E-01	-1.170E+00	-1.115E+00
0.6166	-1.579E-02	-8.504E-03	-7.915E-01	-1.172E+00	-1.116E+00
0.6310	-1.655E-02	-8.631E-03	-7.927E-01	-1.173E+00	-1.116E+00
0.6457	-1.731E-02	-8.759E-03	-7.937E-01	-1.175E+00	-1.116E+00

0.6607	-1.809E-02	-8.885E-03	-7.944E-01	-1.176E+00	-1.116E+00
0.6761	-1.890E-02	-9.005E-03	-7.950E-01	-1.177E+00	-1.116E+00
0.6918	-1.971E-02	-9.125E-03	-7.953E-01	-1.178E+00	-1.116E+00
0.7079	-2.053E-02	-9.244E-03	-7.954E-01	-1.179E+00	-1.115E+00
0.7244	-2.139E-02	-9.354E-03	-7.952E-01	-1.180E+00	-1.114E+00
0.7413	-2.225E-02	-9.464E-03	-7.948E-01	-1.180E+00	-1.113E+00
0.7586	-2.311E-02	-9.573E-03	-7.941E-01	-1.181E+00	-1.112E+00
0.7762	-2.402E-02	-9.672E-03	-7.932E-01	-1.181E+00	-1.111E+00
0.7943	-2.493E-02	-9.770E-03	-7.920E-01	-1.181E+00	-1.109E+00
0.8128	-2.584E-02	-9.868E-03	-7.906E-01	-1.180E+00	-1.108E+00
0.8318	-2.679E-02	-9.953E-03	-7.889E-01	-1.180E+00	-1.106E+00
0.8511	-2.775E-02	-1.004E-02	-7.869E-01	-1.179E+00	-1.103E+00
0.8710	-2.871E-02	-1.012E-02	-7.847E-01	-1.178E+00	-1.101E+00
0.8913	-2.972E-02	-1.019E-02	-7.822E-01	-1.177E+00	-1.099E+00
0.9120	-3.072E-02	-1.026E-02	-7.795E-01	-1.175E+00	-1.096E+00
0.9333	-3.173E-02	-1.033E-02	-7.765E-01	-1.173E+00	-1.093E+00
0.9550	-3.278E-02	-1.039E-02	-7.733E-01	-1.171E+00	-1.090E+00
0.9772	-3.384E-02	-1.044E-02	-7.698E-01	-1.169E+00	-1.087E+00
1.0000	-3.490E-02	-1.050E-02	-7.661E-01	-1.167E+00	-1.083E+00
1.0233	-3.601E-02	-1.054E-02	-7.621E-01	-1.164E+00	-1.079E+00
1.0471	-3.711E-02	-1.058E-02	-7.578E-01	-1.162E+00	-1.076E+00
1.0715	-3.822E-02	-1.062E-02	-7.534E-01	-1.159E+00	-1.072E+00
1.0965	-3.937E-02	-1.065E-02	-7.486E-01	-1.156E+00	-1.067E+00
1.1220	-4.053E-02	-1.068E-02	-7.437E-01	-1.152E+00	-1.063E+00
1.1482	-4.168E-02	-1.071E-02	-7.385E-01	-1.149E+00	-1.058E+00
1.1749	-4.287E-02	-1.072E-02	-7.330E-01	-1.145E+00	-1.054E+00
1.2023	-4.406E-02	-1.074E-02	-7.273E-01	-1.141E+00	-1.049E+00
1.2303	-4.526E-02	-1.075E-02	-7.214E-01	-1.137E+00	-1.043E+00
1.2589	-4.648E-02	-1.076E-02	-7.153E-01	-1.133E+00	-1.038E+00
1.2883	-4.771E-02	-1.076E-02	-7.089E-01	-1.129E+00	-1.033E+00
1.3183	-4.894E-02	-1.077E-02	-7.023E-01	-1.124E+00	-1.027E+00
1.3490	-5.020E-02	-1.076E-02	-6.954E-01	-1.120E+00	-1.021E+00
1.3804	-5.146E-02	-1.076E-02	-6.884E-01	-1.115E+00	-1.015E+00
1.4125	-5.271E-02	-1.075E-02	-6.811E-01	-1.110E+00	-1.009E+00
1.4454	-5.399E-02	-1.074E-02	-6.736E-01	-1.105E+00	-1.003E+00
1.4791	-5.527E-02	-1.072E-02	-6.658E-01	-1.100E+00	-9.960E-01
1.5136	-5.656E-02	-1.071E-02	-6.579E-01	-1.095E+00	-9.893E-01
1.5488	-5.785E-02	-1.069E-02	-6.497E-01	-1.090E+00	-9.825E-01
1.5849	-5.915E-02	-1.067E-02	-6.414E-01	-1.085E+00	-9.755E-01
1.6218	-6.045E-02	-1.065E-02	-6.328E-01	-1.080E+00	-9.683E-01
1.6596	-6.177E-02	-1.062E-02	-6.240E-01	-1.074E+00	-9.610E-01
1.6982	-6.309E-02	-1.059E-02	-6.151E-01	-1.069E+00	-9.535E-01
1.7378	-6.441E-02	-1.056E-02	-6.059E-01	-1.063E+00	-9.459E-01
1.7783	-6.574E-02	-1.053E-02	-5.966E-01	-1.058E+00	-9.382E-01
1.8197	-6.709E-02	-1.049E-02	-5.871E-01	-1.052E+00	-9.303E-01
1.8621	-6.843E-02	-1.046E-02	-5.774E-01	-1.046E+00	-9.222E-01
1.9055	-6.979E-02	-1.041E-02	-5.675E-01	-1.041E+00	-9.140E-01

1.9498	-7.116E-02	-1.037E-02	-5.575E-01	-1.035E+00	-9.057E-01
1.9953	-7.252E-02	-1.032E-02	-5.474E-01	-1.029E+00	-8.972E-01
2.0417	-7.390E-02	-1.027E-02	-5.371E-01	-1.023E+00	-8.886E-01
2.0893	-7.529E-02	-1.022E-02	-5.267E-01	-1.017E+00	-8.799E-01
2.1380	-7.668E-02	-1.016E-02	-5.161E-01	-1.011E+00	-8.711E-01
2.1878	-7.806E-02	-1.011E-02	-5.055E-01	-1.005E+00	-8.621E-01
2.2387	-7.943E-02	-1.005E-02	-4.947E-01	-9.983E-01	-8.530E-01
2.2909	-8.081E-02	-9.992E-03	-4.838E-01	-9.919E-01	-8.438E-01
2.3442	-8.216E-02	-9.934E-03	-4.729E-01	-9.854E-01	-8.345E-01
2.3988	-8.350E-02	-9.876E-03	-4.618E-01	-9.789E-01	-8.250E-01
2.4547	-8.484E-02	-9.818E-03	-4.506E-01	-9.723E-01	-8.154E-01
2.5119	-8.615E-02	-9.761E-03	-4.394E-01	-9.656E-01	-8.058E-01
2.5704	-8.746E-02	-9.706E-03	-4.281E-01	-9.588E-01	-7.960E-01
2.6303	-8.876E-02	-9.650E-03	-4.167E-01	-9.519E-01	-7.861E-01
2.6915	-9.005E-02	-9.596E-03	-4.053E-01	-9.449E-01	-7.761E-01
2.7542	-9.133E-02	-9.544E-03	-3.938E-01	-9.378E-01	-7.660E-01
2.8184	-9.262E-02	-9.491E-03	-3.822E-01	-9.307E-01	-7.558E-01
2.8840	-9.393E-02	-9.440E-03	-3.706E-01	-9.234E-01	-7.455E-01
2.9512	-9.527E-02	-9.391E-03	-3.589E-01	-9.161E-01	-7.352E-01
3.0200	-9.661E-02	-9.341E-03	-3.471E-01	-9.087E-01	-7.247E-01
3.0903	-9.801E-02	-9.292E-03	-3.353E-01	-9.012E-01	-7.141E-01
3.1623	-9.946E-02	-9.244E-03	-3.234E-01	-8.937E-01	-7.034E-01
3.2359	-1.009E-01	-9.196E-03	-3.115E-01	-8.861E-01	-6.927E-01
3.3113	-1.024E-01	-9.148E-03	-2.995E-01	-8.784E-01	-6.818E-01
3.3884	-1.040E-01	-9.101E-03	-2.875E-01	-8.707E-01	-6.709E-01
3.4674	-1.056E-01	-9.054E-03	-2.753E-01	-8.629E-01	-6.598E-01
3.5481	-1.073E-01	-9.007E-03	-2.632E-01	-8.551E-01	-6.487E-01
3.6308	-1.091E-01	-8.960E-03	-2.510E-01	-8.472E-01	-6.375E-01
3.7154	-1.109E-01	-8.913E-03	-2.387E-01	-8.394E-01	-6.262E-01
3.8019	-1.128E-01	-8.865E-03	-2.264E-01	-8.314E-01	-6.149E-01
3.8905	-1.147E-01	-8.818E-03	-2.140E-01	-8.235E-01	-6.034E-01
3.9811	-1.167E-01	-8.771E-03	-2.015E-01	-8.156E-01	-5.919E-01
4.0738	-1.187E-01	-8.723E-03	-1.890E-01	-8.076E-01	-5.803E-01
4.1687	-1.209E-01	-8.674E-03	-1.765E-01	-7.996E-01	-5.686E-01
4.2658	-1.230E-01	-8.626E-03	-1.639E-01	-7.916E-01	-5.568E-01
4.3652	-1.252E-01	-8.577E-03	-1.513E-01	-7.836E-01	-5.450E-01
4.4668	-1.275E-01	-8.528E-03	-1.386E-01	-7.756E-01	-5.330E-01
4.5709	-1.298E-01	-8.478E-03	-1.259E-01	-7.676E-01	-5.210E-01
4.6774	-1.321E-01	-8.428E-03	-1.131E-01	-7.597E-01	-5.089E-01
4.7863	-1.345E-01	-8.376E-03	-1.003E-01	-7.517E-01	-4.968E-01
4.8978	-1.370E-01	-8.325E-03	-8.746E-02	-7.437E-01	-4.845E-01
5.0119	-1.394E-01	-8.273E-03	-7.459E-02	-7.357E-01	-4.722E-01
5.1286	-1.419E-01	-8.218E-03	-6.168E-02	-7.278E-01	-4.598E-01
5.2481	-1.444E-01	-8.164E-03	-4.874E-02	-7.198E-01	-4.474E-01
5.3703	-1.469E-01	-8.109E-03	-3.577E-02	-7.119E-01	-4.348E-01
5.4954	-1.495E-01	-8.051E-03	-2.277E-02	-7.039E-01	-4.222E-01
5.6234	-1.521E-01	-7.994E-03	-9.737E-03	-6.960E-01	-4.095E-01

5.7544	-1.547E-01	-7.935E-03	3.317E-03	-6.881E-01	-3.968E-01
5.8884	-1.572E-01	-7.874E-03	1.639E-02	-6.801E-01	-3.840E-01
6.0256	-1.598E-01	-7.813E-03	2.950E-02	-6.722E-01	-3.711E-01
6.1659	-1.624E-01	-7.751E-03	4.262E-02	-6.642E-01	-3.581E-01
6.3096	-1.650E-01	-7.688E-03	5.576E-02	-6.562E-01	-3.451E-01
6.4565	-1.676E-01	-7.624E-03	6.891E-02	-6.482E-01	-3.320E-01
6.6069	-1.702E-01	-7.560E-03	8.209E-02	-6.402E-01	-3.188E-01
6.7608	-1.728E-01	-7.495E-03	9.527E-02	-6.321E-01	-3.056E-01
6.9183	-1.754E-01	-7.430E-03	1.085E-01	-6.240E-01	-2.923E-01
7.0795	-1.780E-01	-7.365E-03	1.217E-01	-6.158E-01	-2.789E-01
7.2444	-1.806E-01	-7.300E-03	1.349E-01	-6.076E-01	-2.654E-01
7.4131	-1.832E-01	-7.236E-03	1.481E-01	-5.994E-01	-2.519E-01
7.5858	-1.858E-01	-7.171E-03	1.613E-01	-5.911E-01	-2.384E-01
7.7625	-1.885E-01	-7.110E-03	1.745E-01	-5.827E-01	-2.247E-01
7.9433	-1.911E-01	-7.048E-03	1.876E-01	-5.743E-01	-2.111E-01
8.1283	-1.937E-01	-6.987E-03	2.008E-01	-5.658E-01	-1.973E-01
8.3176	-1.963E-01	-6.926E-03	2.139E-01	-5.573E-01	-1.835E-01
8.5114	-1.990E-01	-6.866E-03	2.270E-01	-5.487E-01	-1.696E-01
8.7096	-2.017E-01	-6.805E-03	2.401E-01	-5.400E-01	-1.557E-01
8.9125	-2.044E-01	-6.743E-03	2.531E-01	-5.313E-01	-1.417E-01
9.1201	-2.072E-01	-6.681E-03	2.661E-01	-5.226E-01	-1.276E-01
9.3325	-2.099E-01	-6.619E-03	2.790E-01	-5.138E-01	-1.135E-01
9.5499	-2.128E-01	-6.554E-03	2.919E-01	-5.050E-01	-9.943E-02
9.7724	-2.158E-01	-6.488E-03	3.047E-01	-4.962E-01	-8.528E-02
10.0000	-2.187E-01	-6.423E-03	3.174E-01	-4.874E-01	-7.112E-02
10.2329	-2.218E-01	-6.352E-03	3.301E-01	-4.785E-01	-5.695E-02
10.4713	-2.249E-01	-6.281E-03	3.426E-01	-4.696E-01	-4.279E-02
10.7152	-2.280E-01	-6.210E-03	3.551E-01	-4.608E-01	-2.863E-02
10.9648	-2.312E-01	-6.136E-03	3.674E-01	-4.520E-01	-1.450E-02
11.2202	-2.344E-01	-6.061E-03	3.796E-01	-4.432E-01	-3.989E-04
11.4815	-2.377E-01	-5.987E-03	3.917E-01	-4.344E-01	1.365E-02
11.7490	-2.409E-01	-5.911E-03	4.037E-01	-4.256E-01	2.764E-02
12.0226	-2.442E-01	-5.836E-03	4.155E-01	-4.169E-01	4.156E-02
12.3027	-2.475E-01	-5.760E-03	4.272E-01	-4.083E-01	5.540E-02
12.5893	-2.508E-01	-5.685E-03	4.388E-01	-3.997E-01	6.914E-02
12.8825	-2.541E-01	-5.610E-03	4.501E-01	-3.912E-01	8.278E-02
13.1826	-2.573E-01	-5.534E-03	4.614E-01	-3.827E-01	9.629E-02
13.4896	-2.606E-01	-5.461E-03	4.724E-01	-3.744E-01	1.097E-01
13.8038	-2.638E-01	-5.389E-03	4.833E-01	-3.661E-01	1.229E-01
14.1254	-2.670E-01	-5.316E-03	4.940E-01	-3.578E-01	1.360E-01
14.4544	-2.700E-01	-5.247E-03	5.045E-01	-3.497E-01	1.489E-01
14.7911	-2.731E-01	-5.179E-03	5.148E-01	-3.417E-01	1.617E-01
15.1356	-2.762E-01	-5.110E-03	5.249E-01	-3.337E-01	1.743E-01
15.4882	-2.791E-01	-5.047E-03	5.349E-01	-3.259E-01	1.866E-01
15.8489	-2.820E-01	-4.984E-03	5.446E-01	-3.181E-01	1.988E-01
16.2181	-2.848E-01	-4.922E-03	5.541E-01	-3.105E-01	2.108E-01
16.5959	-2.875E-01	-4.865E-03	5.635E-01	-3.029E-01	2.226E-01

16.9824	-2.902E-01	-4.809E-03	5.726E-01	-2.955E-01	2.341E-01
17.3780	-2.929E-01	-4.753E-03	5.815E-01	-2.882E-01	2.454E-01
17.7828	-2.954E-01	-4.703E-03	5.902E-01	-2.809E-01	2.565E-01
18.1970	-2.978E-01	-4.655E-03	5.986E-01	-2.738E-01	2.674E-01
18.6209	-3.003E-01	-4.606E-03	6.069E-01	-2.667E-01	2.780E-01
19.0546	-3.026E-01	-4.564E-03	6.149E-01	-2.598E-01	2.884E-01
19.4984	-3.048E-01	-4.523E-03	6.227E-01	-2.530E-01	2.985E-01
19.9526	-3.071E-01	-4.483E-03	6.303E-01	-2.462E-01	3.084E-01
20.4174	-3.092E-01	-4.448E-03	6.376E-01	-2.396E-01	3.180E-01
20.8930	-3.112E-01	-4.416E-03	6.447E-01	-2.331E-01	3.274E-01
21.3796	-3.132E-01	-4.383E-03	6.516E-01	-2.267E-01	3.365E-01
21.8776	-3.152E-01	-4.355E-03	6.583E-01	-2.204E-01	3.454E-01
22.3872	-3.171E-01	-4.328E-03	6.647E-01	-2.142E-01	3.540E-01
22.9087	-3.190E-01	-4.301E-03	6.709E-01	-2.082E-01	3.624E-01
23.4423	-3.209E-01	-4.277E-03	6.769E-01	-2.023E-01	3.704E-01
23.9883	-3.227E-01	-4.254E-03	6.826E-01	-1.965E-01	3.783E-01
24.5471	-3.245E-01	-4.232E-03	6.881E-01	-1.908E-01	3.858E-01
25.1189	-3.263E-01	-4.211E-03	6.933E-01	-1.853E-01	3.931E-01
25.7040	-3.280E-01	-4.191E-03	6.984E-01	-1.800E-01	4.002E-01
26.3027	-3.298E-01	-4.171E-03	7.031E-01	-1.747E-01	4.069E-01
26.9153	-3.315E-01	-4.152E-03	7.077E-01	-1.697E-01	4.135E-01
27.5423	-3.331E-01	-4.134E-03	7.120E-01	-1.648E-01	4.197E-01
28.1838	-3.348E-01	-4.116E-03	7.161E-01	-1.600E-01	4.257E-01
28.8403	-3.364E-01	-4.096E-03	7.200E-01	-1.554E-01	4.314E-01
29.5121	-3.380E-01	-4.077E-03	7.237E-01	-1.528E-01	4.369E-01
30.1995	-3.396E-01	-4.057E-03	7.271E-01	-1.503E-01	4.421E-01
30.9030	-3.412E-01	-4.037E-03	7.304E-01	-1.479E-01	4.470E-01
31.6228	-3.427E-01	-4.016E-03	7.334E-01	-1.455E-01	4.517E-01
32.3594	-3.442E-01	-3.995E-03	7.362E-01	-1.431E-01	4.561E-01
33.1131	-3.457E-01	-3.974E-03	7.375E-01	-1.408E-01	4.584E-01
33.8844	-3.471E-01	-3.953E-03	7.388E-01	-1.385E-01	4.605E-01
34.6737	-3.485E-01	-3.931E-03	7.400E-01	-1.362E-01	4.625E-01
35.4813	-3.498E-01	-3.910E-03	7.411E-01	-1.339E-01	4.645E-01
36.3078	-3.511E-01	-3.889E-03	7.423E-01	-1.317E-01	4.665E-01
37.1535	-3.523E-01	-3.869E-03	7.434E-01	-1.294E-01	4.684E-01
38.0189	-3.535E-01	-3.850E-03	7.445E-01	-1.272E-01	4.703E-01
38.9045	-3.545E-01	-3.832E-03	7.456E-01	-1.250E-01	4.722E-01
39.8107	-3.555E-01	-3.815E-03	7.467E-01	-1.228E-01	4.741E-01
40.7380	-3.564E-01	-3.799E-03	7.477E-01	-1.207E-01	4.760E-01
41.6869	-3.572E-01	-3.786E-03	7.488E-01	-1.185E-01	4.778E-01
42.6579	-3.580E-01	-3.772E-03	7.498E-01	-1.164E-01	4.796E-01
43.6516	-3.587E-01	-3.760E-03	7.509E-01	-1.143E-01	4.814E-01
44.6683	-3.592E-01	-3.750E-03	7.519E-01	-1.122E-01	4.832E-01
45.7088	-3.598E-01	-3.740E-03	7.529E-01	-1.102E-01	4.849E-01
46.7735	-3.602E-01	-3.732E-03	7.539E-01	-1.081E-01	4.866E-01
47.8630	-3.606E-01	-3.725E-03	7.548E-01	-1.061E-01	4.883E-01
48.9779	-3.609E-01	-3.719E-03	7.558E-01	-1.042E-01	4.899E-01

50.1187	-3.612E-01	-3.714E-03	7.567E-01	-1.022E-01	4.916E-01
51.2861	-3.613E-01	-3.711E-03	7.576E-01	-1.003E-01	4.932E-01
52.4808	-3.615E-01	-3.708E-03	7.585E-01	-9.841E-02	4.948E-01
53.7032	-3.616E-01	-3.706E-03	7.594E-01	-9.654E-02	4.963E-01
54.9541	-3.616E-01	-3.706E-03	7.602E-01	-9.469E-02	4.978E-01
56.2341	-3.615E-01	-3.705E-03	7.611E-01	-9.287E-02	4.993E-01
57.5440	-3.615E-01	-3.706E-03	7.619E-01	-9.108E-02	5.008E-01
58.8844	-3.612E-01	-3.710E-03	7.627E-01	-8.931E-02	5.022E-01
60.2560	-3.610E-01	-3.714E-03	7.635E-01	-8.757E-02	5.036E-01
61.6595	-3.608E-01	-3.717E-03	7.643E-01	-8.585E-02	5.050E-01
63.0957	-3.607E-01	-3.719E-03	7.651E-01	-8.416E-02	5.064E-01
64.5654	-3.606E-01	-3.722E-03	7.658E-01	-8.249E-02	5.077E-01
66.0693	-3.604E-01	-3.724E-03	7.665E-01	-8.085E-02	5.090E-01
67.6083	-3.604E-01	-3.724E-03	7.673E-01	-7.923E-02	5.103E-01
69.1831	-3.604E-01	-3.724E-03	7.680E-01	-7.763E-02	5.116E-01
70.7946	-3.604E-01	-3.724E-03	7.687E-01	-7.606E-02	5.128E-01
72.4436	-3.604E-01	-3.724E-03	7.693E-01	-7.451E-02	5.140E-01
74.1310	-3.604E-01	-3.724E-03	7.700E-01	-7.299E-02	5.152E-01
75.8577	-3.604E-01	-3.724E-03	7.707E-01	-7.148E-02	5.164E-01
77.6247	-3.604E-01	-3.724E-03	7.713E-01	-7.000E-02	5.176E-01
79.4328	-3.604E-01	-3.724E-03	7.719E-01	-6.855E-02	5.187E-01
81.2830	-3.604E-01	-3.724E-03	7.725E-01	-6.711E-02	5.198E-01
83.1764	-3.604E-01	-3.724E-03	7.731E-01	-6.570E-02	5.209E-01
85.1138	-3.604E-01	-3.724E-03	7.737E-01	-6.430E-02	5.219E-01
87.0963	-3.604E-01	-3.724E-03	7.743E-01	-6.293E-02	5.230E-01
89.1251	-3.604E-01	-3.724E-03	7.749E-01	-6.158E-02	5.240E-01
91.2011	-3.604E-01	-3.724E-03	7.754E-01	-6.025E-02	5.250E-01
93.3254	-3.604E-01	-3.724E-03	7.760E-01	-5.893E-02	5.260E-01
95.4993	-3.604E-01	-3.724E-03	7.765E-01	-5.764E-02	5.270E-01
97.7237	-3.604E-01	-3.724E-03	7.771E-01	-5.636E-02	5.279E-01
100.0000	-3.604E-01	-3.724E-03	7.776E-01	-5.510E-02	5.289E-01

Appendix B: MATLAB Function

The following web link hosts a MATLAB function which implements the model:

https://drive.google.com/open?id=1Af3YLARTYUGuGd12DZ2JbDg41S4fIMJy